Title
THE ABSOLUTE YIELD OF LOW-ENERGY NEUTRONS FROM 190-Mev PROTON BOMBARDMENT OF GOLD, SILVER, NICKEL, ALUMINUM, AND CARBON

Author
Gross, Edward.

Publication Date
1956-02-29

University of California

Ernest O. Lawrence Radiation Laboratory

THE ABSOLUTE YIELD OF LOW-ENERGY NEUTRONS
FROM 190-Mev PROTON BOMBARDMENT
OF GOLD, SILVER, NICKEL, ALUMINUM, AND CARBON

Berkeley, California

DISCLAIMER

UCRL-3330
Physics Distribution

UNIVERSITY OF CALIFORNIA
Radiation Laboratory
Berkeley, California

Contract No. W-7405-eng-48

THE ABSOLUTE YIELD OF LOW-ENERGY NEUTRONS FROM 190-Mev PROTON BOMBARDMENT OF GOLD, SILVER, NICKEL, ALUMINUM, AND CARBON

Edward Gross

(Thesis)

February 29, 1956

Printed for the U.S. Atomic Energy Commission

Contents

THE ABSOLUTE YIELD OF LOW-ENERGY NEUTRONS FROM 190-Mev PROTON BOMBARDMENT OF GOLD, SILVER, NICKEL, ALUMINUM, AND CARBON

Edward Gross

Radiation Laboratory
University of California
Berkeley, California

February 29, 1956

ABSTRACT

The nucleons emitted from high-energy nuclear disintegrations are believed to be the result of a two-stage process: (a) the cascade process followed by (b) the evaporation process. Information concerning the roles of these two processes may be obtained from analyses of the emitted neutron spectra. To this end the differential cross sections for the production of neutrons in the energy interval 0.5 to 12 Mev were measured from C, Al, Ni, Ag, and Au targets at 45°, 90°, and 135° to the 190-Mev proton beam direction. The neutrons were detected by the technique of proton recoils in nuclear emulsions. The internal cyclotron beam was monitored by comparing the activity of foils placed over the target to the activity of foils exposed to the external cyclotron beam. The angular variation of the neutrons emitted from Ag and Au appears to be isotropic in the laboratory. An angular variation begins to appear in the neutrons emitted from Ni and becomes more pronounced in the neutrons emitted from Al and C. Some of the angular variations are consistent with an isotropic center-of-mass distribution, but the angular behavior above a neutron energy of 3 Mev cannot be so interpreted. The observed spectra are therefore attributed to two processes: (a) an isotropic evaporation process, and (b) an angle-dependent cascade process. The total cross section consistent with center-of-mass isotropy is plotted against mass number and compared to similar results from 14-Mev neutron bombardment. The average excitation energy of the evaporating nucleus is plotted against mass number of the target and compared to excitation energies calculated by the Monte Carlo method.

I. INTRODUCTION

The angle and energy distribution of nuclear disintegration products resulting from high-energy nucleon bombardment of nuclei has received much attention both theoretically and experimentally. The nucleonic disintegration products are believed to result from a two-stage process.[1,2] In the first stage the bombarding nucleon is thought to make collisions with individual nucleons or groups of nucleons in the target nucleus, and these in turn to have further collisions within the same nucleus, thus generating a cascade of collisions. Some of the products of these collisions acquire enough energy to leave the nucleus directly, and they leave predominantly in the forward direction. These promptly emitted products constitute the first stage, usually referred to as the cascade stage.

The angle and energy distributions of cascade protons resulting from 90-Mev neutron bombardment of lead were treated theoretically by Goldberger.[3] Goldberger's method has subsequently been expanded by Bernardini et al.[4] and by McManus and Sharp.[5] Goldberger treats the target nucleus as a degenerate Fermi gas and uses experimentally determined differential cross sections to treat nucleon-nucleon collisions within the nucleus. He then uses the Monte Carlo method to trace the path of a nucleon through the target nucleus, and thus develops the cascade.

At the end of the cascade stage ($\sim 10^{-22}$ sec) a residual nucleus remains which is usually in a highly excited state. Further particle emission can then follow by the comparatively slower second phase, the evaporation process.[6] In this stage it is assumed that the excess energy is quickly shared among the remaining nucleons and that many collisions with the nuclear surface occur before a particle is emitted. In this time ($\sim 10^{-20}$ sec), the many nucleon collisions result in an angular distribution that is symmetric about 90° in the center-of-mass of the emitting nucleus.[7] If many angular momentum states are present, the angular distribution is expected to be isotropic. The energy distribution of products resulting from the evaporation process was obtained

by Weisskopf,[6] who introduced the idea of nuclear temperature to characterize the excited nucleus. His ideas were expanded and improved by Bagge,[1,8] who made allowance for cooling following particle emission, and by LeCouteur,[9] who made allowance for the thermal expansion of the nucleus and extended the theory to very high excitation energies.

In general, the evaporation products are expected to have an isotropic center-of-mass distribution and an energy spectrum that is highly peaked at low energies. The cascade products are characterized by an angular distribution that increases towards the beam direction and has a very broad energy distribution extending to the highest energies compatible with the bombarding conditions.

These features of high-energy nuclear disintegration have, to some extent, been experimentally verified for the charged particles resulting from nuclear breakup. Harding, Lattimore, and Perkins[10] analyzed the energy and angular distributions of singly and doubly charged particles from stars produced by cosmic rays in the heavy nuclei of emulsion. They found very good agreement with the predictions of evaporation theory for protons less than 30 Mev. They also found a high-energy tail that had a forward rise in its angular distribution suggestive of the cascade process. Perkins[11] extended this analysis to those stars with excitation energies greater than 700 Mev, and still found very good agreement with the evaporation theory as amended by LeCouteur.[9]

Similar experiments have been carried out, using machine-produced particles to bombard emulsion. Bernardini, Booth, and Lindenbaum,[12] using 450-Mev protons and 300-Mev neutrons, and Lock, March, and McKeague,[13] using 950-Mev protons to bombard the heavy nuclei of emulsion, also found general agreement with the two-step process but found a higher percentage ($\sim 25\%$) of cascade protons in the evaporation energy region than in the experiments done with cosmic rays at higher energies. This result may be due to the higher excitation energies available at cosmic-ray bombarding energies. As the excitation energy is increased, the energy interval

containing the cascade particles is also increased. On the other hand, a comparison of the results at high excitation energy,[10,11] with the results at comparatively low excitation energy[12] reveals that the energy interval containing the evaporation particles changes very little over very large variations in excitation energy. The yield of cascade particles relative to that of evaporation particles in the evaporation energy region is thus expected to decrease as the excitation energy increases until this yield is undetectable at cosmic-ray energies.

Experiments using pure elements rather than emulsion as a target also verify the two-step process as well as give specific information on variations with atomic number. Gugelot[14] bombarded various targets with 18-Mev protons and examined the angle and energy distribution of the inelastically scattered protons. His results show general agreement with the evaporation theory for the lower-energy protons from the elements Al, Fe, Ni, and Cu. The higher-energy protons showed a forward rise in the angular distribution. For Ag, and elements of higher atomic number, even the low-energy protons exhibit an angular distribution that increases toward the beam direction. Bailey,[15] using 190-Mev protons to bombard C, Al, Ni, Ag, and Au targets, has measured the energy spectra, the angular variations, and the yields of protons, α particles, deuterons, tritons, and He^3 nuclei emitted by these targets. He finds evaporation-type spectra for the low-energy protons (less than 30 Mev) resulting from bombardment of elements through Ag. The protons with energies above 30 Mev have a yield higher than that expected from evaporation theory, and an angular distribution suggestive of the cascade effect. The protons from Au appeared to be entirely of the cascade type. Bailey also found that the yield of low-energy protons did not increase monotonically with increasing atomic number. This yield increased from C to Ni but decreased in going from Ni to Au.

The behavior of the proton energy spectra as a function of atomic number observed by Gugelot[14] and by Bailey[15] may be understood as being a Coulomb barrier effect. For a moderate excitation energy there will be a Coulomb barrier high enough to considerably suppress low-energy charged-particle evaporation. For nuclei with higher Coulomb barriers, the only way to obtain a low-energy charged particle is by a direct knockout process. For higher excitation energies, a higher Coulomb barrier is needed to suppress the evaporation yield of charged particles. This would explain the evaporation proton spectra resulting from 190-Mev proton bombardment of Ag,[15] and the appearance of a considerable cascade production of protons for the same element at 18-Mev proton bombardment.[14]

To help complete the picture of nuclear breakup, knowledge of the behavior of the emitted neutrons is desired. Neutron data also have the advantage of not being complicated by a Coulomb barrier, and thus may be more easily compared to theoretical predictions. Gugelot[16] has obtained the neutron spectra at zero degrees resulting from 16-Mev proton bombardment of various elements. The shape of his spectra agrees well with evaporation theory, but his nuclear temperatures varied surprisingly little throughout the periodic table. Graves and Rosen,[17] using 14-Mev neutrons to bombard various elements, also report agreement of the resulting neutron-energy spectra with evaporation theory, but only for neutrons with energies less than 4 Mev. Above this energy the neutron yield is higher than predicted by evaporation theory. They also find temperatures in agreement with Gugelot,[14, 16] and a yield that increases with atomic number. Skyrme and Williams[18] report the absolute yield of neutrons in the energy region 0 to 12 Mev at 180° to the 150-Mev proton bombardment of tungsten and carbon. The spectrum from tungsten is said to be in agreement with evaporation theory, but the carbon data are complicated by a probable center-of-mass motion of the evaporating nucleus. The existence of neutrons in the cascade energy region is verified by the experiments of Hofmann and Strauch,[19] who examined neutron yields from various targets in the energy region 50 to 100 Mev resulting from 95-Mev proton bombardment.

The work reported herein gives the absolute yield of neutrons from C, Al, Ni, Ag, and Au targets at 45°, 90°, and 135° to the 190-Mev proton beam direction, as well as their energy spectra in the region 0.5 to 12 Mev. The work of Graves and Rosen[17] is thus extended to higher bombarding energies, where the cascade production of neutrons becomes more important. An angular distribution of the resulting neutrons is obtained to help determine the relative importance of the cascade and evaporation processes in this energy region. It is hoped that the yield of neutrons together with the yield of charged particles from the same targets under similar bombarding conditions,[15] will result in a more complete picture of nuclear breakup.

II. EXPERIMENTAL ARRANGEMENT

The 190-Mev proton bombardments were achieved by placing targets at the 60-inch radius of the 184-inch cyclotron. The spread in beam energy is estimated to be ± 15 Mev.[20] To detect the resultant low-energy neutrons, the method of proton recoils in emulsion was used.[21]

The apparatus used to make the emulsion exposures consisted of a target holder, shielding, and emulsion plate holder (Fig. 1). The target holder and shielding was constructed as a single rigid unit that would fit on the proton probe cart of the 184-inch cyclotron. The proton probe cart can enter the cyclotron vacuum tank through an air lock and the cart can be positioned at a desired radius between the magnet pole faces.

The emulsion plate holder and the shielding consisted of three narrow channels cut into brass at 135°, 90°, and 45° to the direction of the proton beam at the target. Plates were held in position by means of double-surfaced Scotch Tape on one of the walls of each channel. The 135° and 90° emulsion plates began 6 inches from the target and extended to 9 inches from the target. To reduce charged-particle background, it was found necessary to start the 45° plate 8 inches from the target. When in place, the emulsion was perpendicular to the median plane of the cyclotron, and this plane bisected the 1-inch side of the 1- by - 3-inch plates. A charged particle of medium energy originating at the target and entering one of the channels is bent away from the emulsion surface and into the channel walls by the magnetic field of the cyclotron. Neutrons pass down the channel undeflected by the magnetic field and enter the emulsion surface at a small angle to this surface ($\sim 2^{\circ}$). The channel and shielding began at a radius 3 inches greater than that of the target. Beam clippers were placed at a radius 1.5 inches greater than the target and were positioned as indicated in Fig. 2.

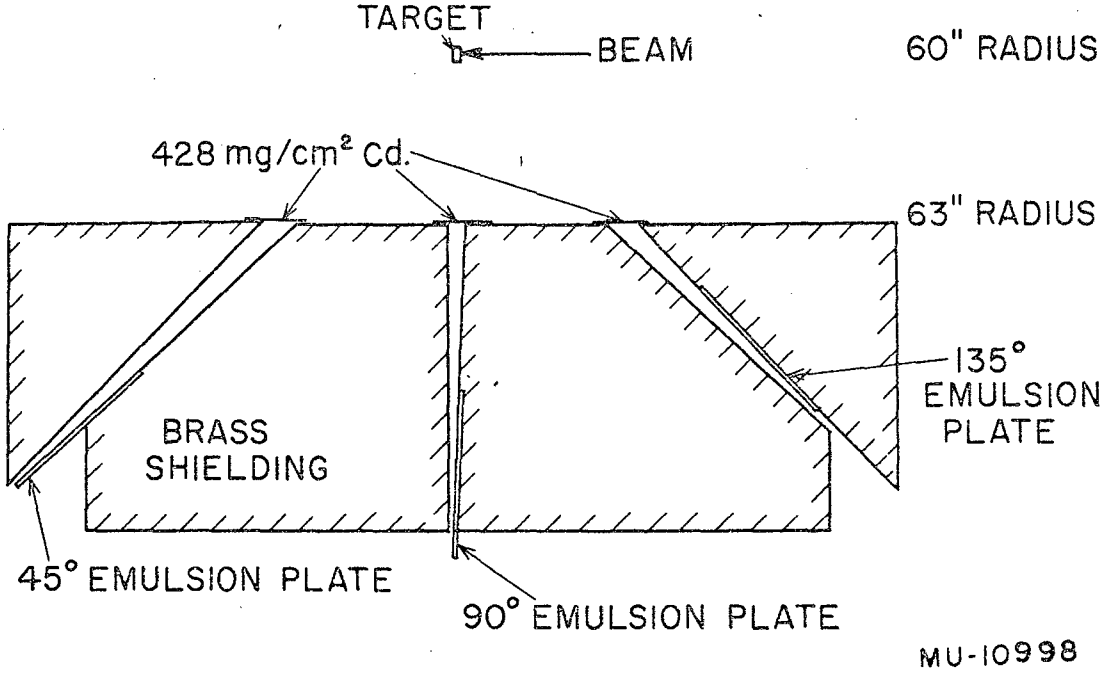

Fig. 1. Arrangement of target, shielding, and nuclear emulsion plates inside the vacuum tank of the 184-inch cyclotron.

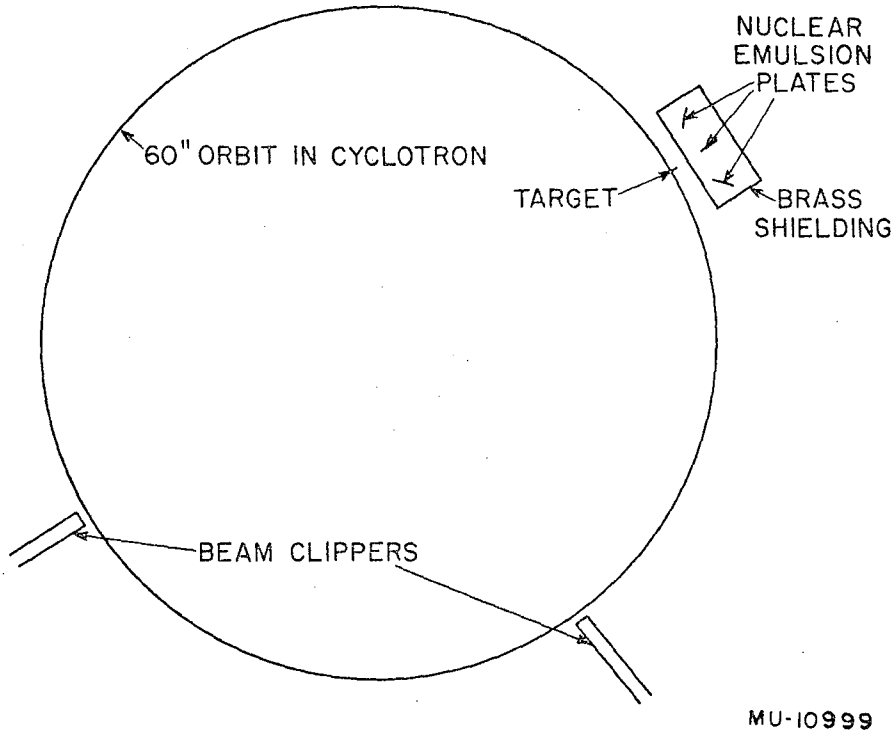

Fig. 2. Radial relationship of beam clippers, target, shielding, and nuclear emulsion plates between the magnet pole faces of the 184-inch cyclotron.

The target holder was made of dural and it gripped the target at a point 4.5 inches below the center of the beam. Final alignment of the target was determined by sighting down each channel from the position of the emulsion.

To position the target and beam clippers radially, a current-reading probe was used to record beam current as a function of radius. Figure 3 is a plot of beam current versus radius when the beam clippers were in place. The radial position of the shielding with respect to the beam clippers is also indicated in Fig. 3.

When the beam clippers were positioned, the target was inserted in the target holder and aligned. The emulsion plates were then positioned in the channels. To better position the emulsion plates, they were not wrapped in the usual black paper but were positioned bare. During the positioning stage the cyclotron lights were turned off. To protect the emulsions from being light struck in case of the possible arcing of the cyclotron, a 428-mg/cm^2 strip of cadmium was placed over the entrance to each channel. The proton probe cart then entered the cyclotron and was positioned at the desired radius by remote control. After the cyclotron had been sufficiently pumped down, an exposure was made. The exposure finished, the cart was removed from the cyclotron to the air lock, the air lock was then let down to air, the cart extracted, and the emulsion plates removed to a dark box. The lights were then turned on and the target was removed to safe storage until needed for beam monitoring.

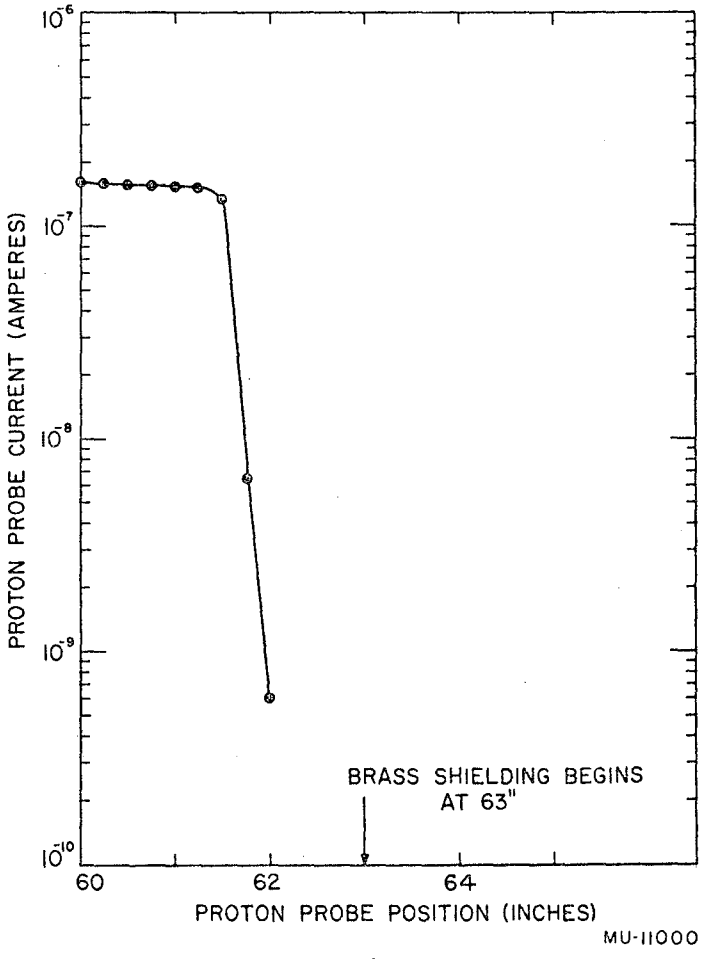

Fig. 3. Proton probe current as a function of cyclotron radius when the target is out and the beam clippers are in place.

III. DETERMINATION OF THE ABSOLUTE CROSS SECTION

A. The Cross-Section Formula

Let $\frac{d\sigma}{dE_n d\Omega}(z, E_n, \theta)$ be the cross section per unit energy interval, per unit solid angle, for obtaining neutrons of energy E_n at the angle θ, from a target of element z. If $N_{T,z}$ beam protons pass through a target of element z, whose thickness in the beam direction is $x_{T,z}$ nuclei/cm^2, then the yield of neutrons per unit energy interval per unit solid angle, $\frac{dN_n}{dE_n d\Omega}(z, E_n, \theta)$, is given by

$$\frac{dN_n}{dE_n d\Omega}(z, E_n, \theta) = N_{T,z}\, x_{T,z}\, \frac{d\sigma}{dE_n d\Omega}(z, E_n, \theta). \qquad (1)$$

The neutrons from the target now constitute a new beam and the protons in the emulsion constitute a new target. Let $\sigma_{np}(E_n)$ be the total cross section for a neutron-proton collision for neutrons of energy E_n. If $N_n(E_n)$ neutrons of energy E_n pass through a proton target of density ρ_p protons/cm^3 and thickness t_e in the neutron direction, there will be produced $N_p(E_n)$ proton recoils, given by

$$N_p(E_n) = N_n(E_n)\, \rho_p\, t_e\, \sigma_{np}(E_n). \qquad (2)$$

Combining Eqs. (1) and (2), we get

$$\frac{d\sigma}{dE_n d\Omega}(z, E_n, \theta) = \frac{1}{N_{T,z}\, x_{T,z}\, \rho_p\, \sigma_{np}(E_n)}\, \frac{dN_p}{dE_n\, dV/r^2}(z, E_n, \theta), \qquad (3)$$

where $t_e d\Omega$ has been replaced by dV/r^2. Here dV is the emulsion volume scanned for proton recoil events and "r" is the distance of this volume from the target.

It is seen from Eq. (3) that a determination of the absolute cross section requires a determination of the quantities $x_{T,z}$, $N_{T,z}$, ρ_p, dN_p/dE_n, and dV/r^2. The determination of each of these quantities will be discussed. The values of the proton-neutron collision cross section, $\sigma_{np}(E_n)$, have been taken from the review article by Adair.[22]

B. Targets

Background that builds up with exposure time and does not depend on target thickness can be reduced by choosing a thicker target. Some of the background in this experiment seemed to be of this nature. However, a target should not be thick enough to cause serious absorption of neutrons within the target itself. With these considerations in mind, the following target thicknesses were used:

Target	Radial thickness (nuclei/cm^2)	Thickness along beam (nuclei/cm^2)	Beam energy loss (Mev)
C	5.45×10^{22}	5.55×10^{22}	4.7
Al	3.75×10^{22}	4.08×10^{22}	6.2
Ni	5.80×10^{22}	2.96×10^{22}	7.3
Ag	3.73×10^{22}	1.90×10^{22}	9.6
Au	3.82×10^{22}	9.92×10^{21}	14.6

All thicknesses were determined to within 1/2 %.

C. Monitoring of the Beam

To find the number of protons that went through each target, the following method was employed. Thin foils of the target material were placed on the front and back faces of the target. The front of the target faces the beam. Care is taken to make sure that the edges of each foil coincide with the edges of the target, then the beam that passes through the target also passes through the foils. For the carbon target, polyethylene foils were used. Following a cyclotron run, the foils were monitored by centering the active region of each foil on the axis of a thin-window Geiger tube at a reproducible distance from the window. Next, a multiple sandwich was made of all the foils, including guard foils for each element, clamped between two strips of 1/16-inch dural. Each edge of the sandwich was milled. This sandwich was exposed at the same cyclotron radius as the previous target exposures and in such a manner that the same beam passes through all the foils. Each foil from the sandwich exposure was then monitored in the same geometry and at the same time after exposure as were the corresponding foils from the previous target exposures. Finally a known number of 340-Mev protons were passed through polyethylene foils from the external cyclotron beam; a Faraday cup was used to collect this beam. The number of protons through a target exposure of element z, $N_{T,z}$ is then given by

$$N_{T,z} = \frac{\sigma_{e,c}}{\sigma_{s,c}} \frac{\Delta t_{T,z}}{\Delta t_{e,c}} \left[\frac{1-e^{-\Delta t_{e,c}/\tau_c}}{1-e^{-\Delta t_{s,c}/\tau_c}}\right]\left[\frac{1-e^{-\Delta t_{s,z}/\tau_z}}{1-e^{-\Delta t_{T,z}/\tau_z}}\right] \times$$

$$\frac{A_{s,c}(t_s = t_e)}{A_{e,c}(t_s = t_e)} \frac{A_{T,z}(t_{T,z} = t_{s,z})}{A_{s,z}(t_{T,z} = t_{s,z})} N_{e,c} , \qquad (4)$$

where $A_{i,z}(t_i)$ is the activity in counts/min/mg/cm^2 of a foil of element z, at a time t_i after its exposure. Here subscript "i" can be any of the following symbols indicating the type of exposure:

T is a target exposure,

s is a sandwich exposure,

e is an external beam exposure.

The expression $\Delta t_{i,z}$ is the time that the beam is on during type "i" exposure of element z. The term $\tau_{i,z}$ is the measured mean life of the activity produced by bombarding element z. z = c refers to polyethylene foils. $\sigma_{i,c}$ is the cross section for making the C^{11} activity used to monitor the polyethylene foils. These values were taken from Crandall et al.[23]

The main uncertainty in $N_{T,z}$ comes from an uncertainty in the centering of each foil. It is estimated that this uncertainty is about 0.25 inch. From a knowledge of the variation in counting rate as a function of the distance of a point source from the tube axis, it is found that a foil that is off center by 0.25 inch will have about a 10% smaller counting rate than it would have if it were centered. The sandwich exposure was repeated three times with consistent results. The ratio of two activities in the sandwich exposure is believed to be accurate to within 2%. Other uncertainties in the value of $N_{T,z}$ include a 1% uncertainty in the density of each foil, an uncertainty of 3% in $\frac{\sigma_{e,c}}{\sigma_{s,c}}$[23], an uncertainty of 2% in integration of the external beam, and an uncertainty of 2% introduced by an uncertainty of 0.1 minute in the mean life of the C^{11} activity. The total estimated error in $N_{T,z}$ is then about 18%.

D. Shrinkage Factor and Hydrogen Density of the Emulsions

Ilford C.2 emulsions have sufficient sensitivity to distinguish between singly and doubly charged particles of about nucleon mass and low velocities, and they are not sensitive enough to be troubled by the large electron background encountered in an internal cyclotron exposure. Emulsions 200μ thick were chosen because these were sufficiently thick for the proton ranges encountered in this work. This thickness of emulsion can also be conveniently processed at room temperature.[24]

It is important to know the factor by which an emulsion shrinks because of processing. This shrinkage factor allows conversion of space angles measured in the processed emulsion to space angles in the unprocessed emulsion. The emulsion is constrained from shrinking laterally by glass backing, and, except for the edges, the shrinkage is in the vertical direction and is uniform throughout the emulsion volume.[25]

To determine this shrinkage factor, the following method was employed. A dial gauge was used to measure the thickness of emulsion plus glass, both before and after processing. Care was taken to make measurements at the same point. The processed emulsion thickness at this point was readily obtained by using the vertical focus of a microscope. The vertical control was found to be linear and its calibration was checked to less than 1%. Using this method on 15 emulsions processed together yielded the result $s = 2.17 \pm 0.04$ for the shrinkage factor. The shrinkage factor was found to vary less than the stated uncertainty over the range of relative humidities (35% to 65%) that were encountered in the scanning of the emulsions.

Recent measurements of the hydrogen density as a function of relative humidity for Ilford emulsion have been made by Waller.[26] The new measurements are stated to have an accuracy of 2%. It should be noted that the new determination of the hydrogen density at 0% relative humidity is about 10% lower than the old value quoted by Ilford Ltd.

The 200-μ Ilford C.2 emulsions used in this experiment were kept in an atmosphere of about 50% relative humidity for a week before they were used in the cyclotron. The desired relative humidity was attained by use of a suitable mixture of glycerine and water.[27] A control plate was weighed both before and after each cyclotron exposure. The control plates were then dried by heating to 110°C in an oven, and again they were weighed to determine the amount of water driven out of each emulsion. The emulsions were then stripped from their glass plates and each glass plate was weighed. Knowing the weight of each glass plate and the weight of water driven out of each emulsion, one can calculate the fraction by weight of each emulsion that is water.

The fractional water content, together with the density of dry emulsion, allows calculation of the density of the emulsion at the time of exposure.[28] The results obtained in this way agreed within 2% with the density expected for emulsion at 50% relative humidity.[26,27] On the basis of Waller's data,[26] an uncertainty of 2% in emulsion density introduces an uncertainty of 4% in the hydrogen density at 50% relative humidity.

E. Method of Scanning

The important quantity obtained from the scanning is the number of proton recoils per neutron energy interval per unit volume of emulsion scanned, $\frac{dN_p}{dE_n dV}$. This quantity is directly related to the neutron cross section per neutron energy interval per steradian by Eq. (3).

To make the necessary measurements the emulsions were scanned with binocular microscopes using 90- and 45-power oil-immersion objectives and 10-power eyepieces. The 45-power objective was used when it was necessary to build up statistics on the long-range proton recoils (30 microns or more). Sweeps were taken along the 1-inch direction of the emulsion, all events in this sweep occuring at the same distance from the target. One eyepiece was fitted with a graduated reticle and goniometer which served to define the scanning area and to measure the projected range and projected angle of the events. The position of the sweep relative to the edges of the nuclear emulsion plate was accurately fixed by a calibrated microscope stage. Dip measurements were made by a fine-focus vertical control calibrated in 1-micron units. The fine-focus vertical control, together with the reticle and the calibrated microscope stage, determines the volume of emulsion scanned.

Events are obtained by scanning for tracks that end in the field of view and which lie no closer than 2 microns to the top or bottom surface of the emulsion. The beginning of the track is then examined by moving the stage and vertical focus. The beginning must also be more than 2 microns from the top or bottom surface of the emulsion. The track must not be a star prong or connected to a recoil nucleus.

Occasionally tracks are found that begin and end within the emulsion and are not connected with stars or recoils but, from the appearance of the track, obviously have a charge greater than that of the proton. Such events are not recorded. If a track meets the above criteria, it is judged a proton recoil. Protons, deuterons, and tritons from (n, p), (n, d), and (n, t) reactions within the emulsion also have the appearance of a proton recoil. It is estimated, however, that this source of background contributes less than 5% to the true number of proton recoils per neutron energy interval.[29]

To be accepted for measurement, a proton recoil must meet one further requirement; it must lie within a 20° cone about the neutron direction from the target. The cone angle refers to the unprocessed emulsion. There are three reasons for this requirement: (a) the energy resolution suffers for steeply dipping tracks because range and angle measurements are more uncertain for these tracks; (b) corrections for leaving the emulsion are more serious for steeply dipping tracks; and (c) the direction of travel of the proton becomes more uncertain for steeply dipping tracks. The directional property of proton recoils is useful in background determinations. A 20° cone offers satisfactory energy resolution for this experiment. It has the advantage over smaller cones in reducing the scanning time necessary to obtain any desired statistics. A 20° cone also has a smaller solid-angle error than would a smaller cone, and is thus more suited to an absolute cross section measurement (see Appendix I).

The solid angle scanned for events is determined by (a) the requirement that events lie within a 20° cone, together with (b) the volume (before processing) of the emulsion that is scanned. Neutron-proton collisions are known to have isotropic center-of-mass distributions up to 3.3 Mev[30] and to be less than 5% anisotropic at 14 Mev.[31] If the center-of-mass distribution is isotropic, proton recoils have a distribution in the laboratory system given by

$$P(\theta)\, d\theta = \sin 2\theta\, d\theta, \qquad (5)$$

where θ is the angle between the proton direction and the initial neutron direction. Accepting only events for which $\theta \leq 20^{\circ}$ results in a fraction of the total solid angle given by

$$f(20^{\circ}) = \frac{\int_0^{20^{\circ}} \sin 2\theta \, d\theta}{\int_0^{\pi/2} \sin 2\theta \, d\theta} = 1/2 \left[1 - \cos 40^{\circ}\right] = 0.117 . \qquad (6)$$

The solid angle scanned for events is therefore given by $dV/r^2 t_e \times 0.117$.

For the neutrons entering the emulsion at a grazing angle, the space angle θ between a neutron and its proton recoil is given by

$$\cos \theta = \cos \alpha \cos \beta, \qquad (7)$$

where α is the projected angle of the proton recoil in the plane of the emulsion and β is the dip angle of the proton recoil in the unprocessed emulsion. It is then required that each event have both α and β less than or equal to 20° in order to meet the requirements $\theta \leq 20^{\circ}$. In reducing the data, only those tracks for which $\arccos(\cos\alpha \cos\beta) \leq 20^{\circ}$ are accepted.

When an event is found that satisfies the above criteria, the following measurements are made upon the track:

(a) The x axis of the reticle is aligned with the beginning straight section of the track. The projected angle α of the track with respect to the x axis (the neutron direction) is then read to 0.1° from the goniometer, and recorded.

(b) The projected range of the first straight section of track, r_H, is measured to 0.1 reticle unit and recorded. (One reticle unit is about one micron.)

(c) This straight section is then centered in the field of view with the first grain in sharp focus. This z coordinate is read and recorded to 0.1 micron from the fine focus. This is repeated for the last grain of the straight section (with the slack always taken out of the fine focus in the same direction). The difference between these measurements, Δz, is the dip for r_H reticle units.

(d) The total projected range of the track, R_H, is then measured and recorded to within 0.1 reticle unit.

(e) It is also noted whether the proton recoil is going towards the target or away from the target, or whether its direction is unknown. This last piece of information is useful in correcting the data for background.

The accuracy to which the various microscope measurements can be made, together with the number of events found, determines the error in the quantity

$$\frac{\Delta N_p}{\Delta E_n \Delta V / r^2 f(\theta)},$$

which is related to the absolute cross section by Eq. (3).

For estimation of the errors in the above quantity, root-mean-square deviations of various quantities measured by use of the microscope have been determined. These include a 2% error in the shrinkage factor, a 0.5% error in the reticle calibration, a 0.5° error in the projected angle, and an error of 0.25 micron in the dip of a track. The uncertainty in the emulsion volume is then about 3%. Owing to an uncertainty in the radial distribution of the beam at the target, the error in r^2 is estimated to be about 3%. The energy of an individual neutron may be in error by about 3% (see Appendix 2). The error in the energy interval ΔE_n is negligible, however, because the number of neutrons whose true energies lie outside of this energy interval but which are measured as lying within the interval should approximately equal the number of neutrons whose true energies lie within the energy interval but which are measured to lie outside of the interval. The error in the solid-angle factor $f(\theta)$ depends on the accuracy of measuring space angles θ, in the neighborhood of $\theta = 20^\circ$ (see Appendix 1). The standard deviation of θ near $\theta = 20^\circ$ was found to lie between 0.5° and 3°, depending on the range of the track measured. The shorter the track, the larger the uncertainty in its space angle θ. However, aside from the variation of events in space angle (Eq. (5)), the number

of tracks that actually lie outside the cone but which are measured to lie inside the cone should approximately equal the number of tracks that actually lie inside the cone but which are measured as lying outside the cone. If the error in measuring the space angle is large, then the variation of proton recoils with space angle (Eq. (5)) is expected to affect the efficiency for observing these recoils in a particular cone. This effect is not important above a neutron energy of 0.5 Mev.[32] Aside from the statistical error in N_p, the error in

$$\frac{\Delta N_p}{\Delta E_n \Delta V / r^2 f(\theta)}$$

is then about 4% and the error in the differential cross section is about 20%.

IV. REDUCTION OF THE DATA

As explained in the previous section, microscope measurements are made on each proton recoil to determine its horizontal projected angle α, its vertical dip Δz for r_H reticle units of projected range, and its total projected range R_H, in reticle units. The space angle in the unprocessed emulsion between the neutron and its proton recoil may then be determined by Eq. (7), where the cosine of the dip angle β is given by

$$\cos \beta = \cos \left[\tan^{-1} (s\Delta z / k r_H) \right], \tag{8}$$

where s is the shrinkage factor and k is the reticle calibration in microns per reticle division. Only events having $\theta \leq 20^{\circ}$ are accepted for analysis. If the measurements are made correctly, the distribution of events in space angle should be given by Eq. (5). Figure 4 is an example of the observed distribution of events with space angle.

The range of the proton recoil can be calculated from

$$R_p = k R_H / \cos \beta . \tag{9}$$

Referring to the range-energy relation for protons in emulsion,[33] one can obtain the energy of the proton recoil, E_p, whose range is given by Eq. (9). The energy of the neutron, E_n, that produced a proton recoil of energy E_p at the angle θ is given by

$$E_n = E_p / \cos^2 \theta . \tag{10}$$

About half of these tedious calculations were coded for machine calculation (IBM 650). For machine calculation, Eq. (10) was replaced by

$$E_n = \frac{a + b R_p^{1/2} + c R_p}{\cos^2 \theta}, \tag{11}$$

where a, b, and c are chosen to fit the range-energy relation.[33] For $R_p \geq 80$ microns the values for a, b, and c have been taken from Rosen:[29]

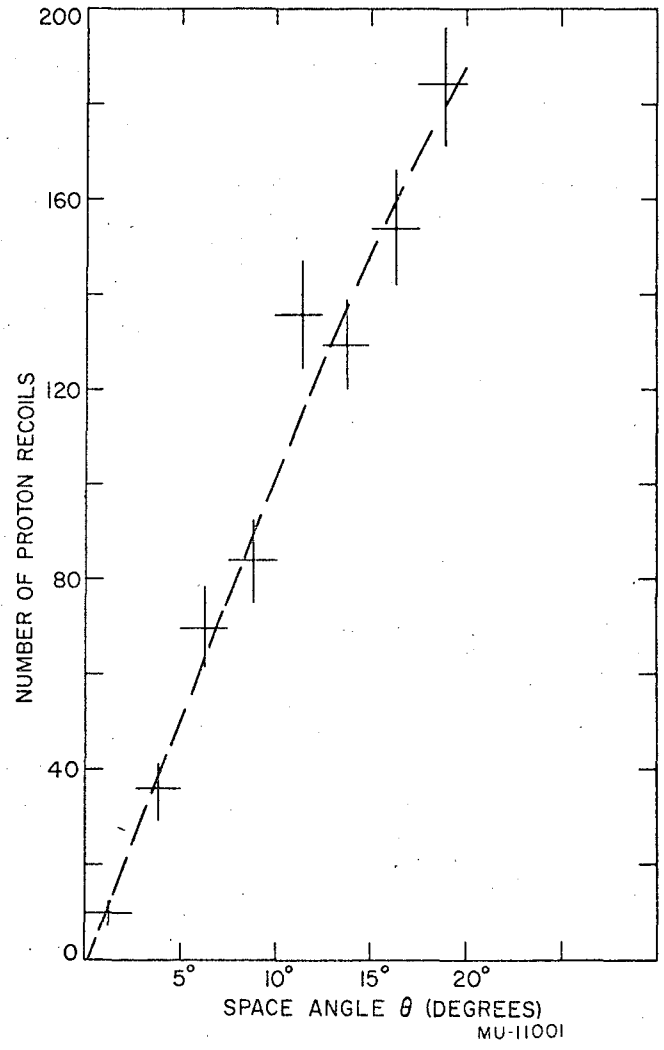

Fig. 4. The observed angular distribution of proton recoils with respect to the neutron direction. The broken curve represents the expected distribution (Eq. (5)) normalized to the total number of events (803).

$a = -0.47$,

$b = 0.381$ (for $R_p \geq 80$ microns),

$c = 0.002778$.

For $R_p \leq 80$ microns the following values were found to be a good fit:

$a = -0.189$,

$b = 0.263$ (for $R_p \leq 80$ microns),

$c = 0.013$.

These constants fit the range-energy relation to within less than 2%.

The events are then broken down into suitable energy intervals and the number of proton recoils in a 20^{o} cone, per neutron energy interval, per unit volume of emulsion $\dfrac{\Delta N_p}{\Delta E_n \Delta V / r^2 f(\theta)}$, is obtained. This quantity is then used to calculate the absolute differential cross section given by Eq. (3). The middle point of the energy interval ΔE_n was used to choose the value of the total neutron-proton collision cross section, $\sigma_{np}(E_n)$, to be used in Eq. (3). This value of $\sigma_{np}(E_n)$ differs by less than 2% from the value obtained by using the mean energy of the interval calculated from the observed energy spectrum.

V. CORRECTIONS TO THE DATA

A. Scanning Efficiency

The scanning must be checked both for correctness of track measurements and for efficiency of finding events. If the track measurements are made correctly then the distribution of proton recoils in space angle should be $\sin 2\theta \, d\theta$. Figure 4 is a typical example of the space-angle distribution obtained by one of the scanners. A similiar check can be made on the distribution of events in the plane perpendicular to the neutron direction. Events should be distributed at random in this plane. Figure 5 is a typical example of the distribution of events in azimuthal angle.

The efficiency for finding events may be obtained by having two scanners scan the same volume of emulsion. Scanner No. 1 finds N_1 events in a 20° cone and scanner No. 2 finds N_2 events in a 20° cone. Let $N_{1,2}$ be the number of events found by scanner No. 1 that scanner No. 2 found in a 20° cone. Not all the $N_{1,2}$ events need lie inside the 20° cone. Then scanner No. 1's efficiency is given by

$$e_1 = N_{1,2}/N_2 \, . \tag{12}$$

Likewise,

$$e_2 = N_{2,1}/N_1 \, . \tag{12'}$$

The efficiencies found in this way ranged between 0.9 and 1.0.

B. Background Correction

The presence of neutron sources other than the target is evident from the observation of proton recoils going in the direction toward the target. As explained earlier, data are gathered by recording proton recoils that lie within a 20° cone about the neutron direction from the target. It is evident that neutrons directly from the target cannot produce proton recoils that are traveling toward the target. Neutrons inelastically scattered from the brass shielding about the plates can produce such recoils, and so can neutrons resulting from stray beam hitting the brass shielding and iron pole faces. Such neutrons result from compound-nucleus formation, and are essentially isotropic.

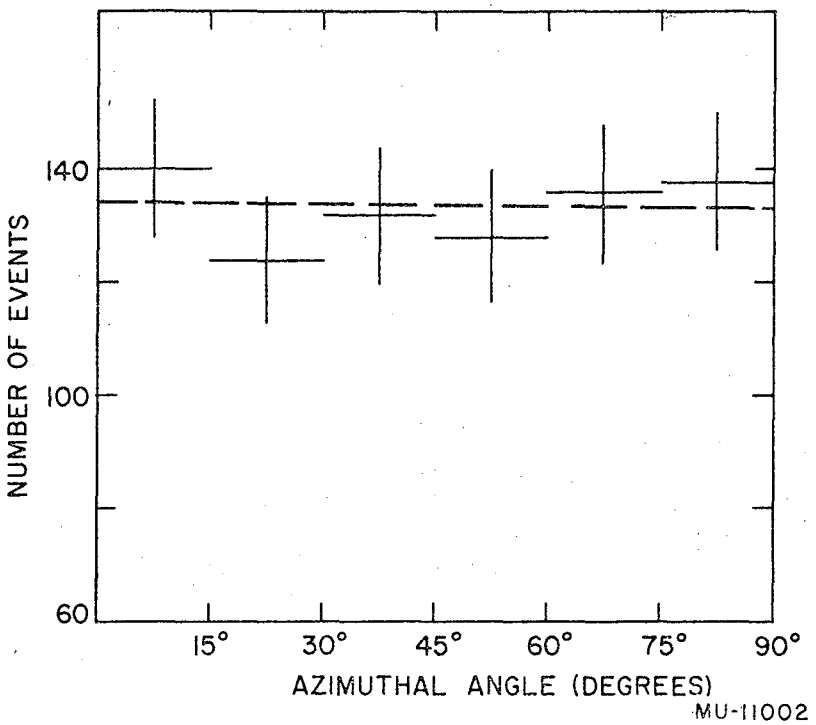

Fig. 5. The observed angular distribution of proton recoils in the plane perpendicular to the neutron direction. Events from all four quadrants are combined. The broken line represents the expected random distribution of events in this plane.

The number of proton recoils traveling towards the target and lying within a 20^{o} cone is then a measure of the proton recoils in the forward 20^{o} cone that are due to neutrons from other sources than the target. Cones of 20^{o} at various angles in the backward hemisphere were scanned for proton recoils, and the results are consistent with spherical symmetry.

The direction of a proton recoil is ascertained by the increase of ionization and scattering at the end of its range. The track must be long enough, however, for these changes to be self-evident. The length of proton track necessary for direction determination was obtained by recording for each event whether or not its direction was certain. Figure 6 is a plot of the observed percent certainty versus neutron energy interval for one of the scanners. It is evident that above 1.75 Mev the direction of a proton recoil is virtually certain. The energy spectrum of the proton recoils above 1.75 Mev and going toward the target within a 20^{o} cone about the neutron direction from the target is presented in Fig. 7. This spectrum is in agreement with the average proton recoil spectrum observed from Ni, which is also presented in Fig. 7. This would be expected if the sources of the background were stray beam and neutrons hitting the magnet pole faces and the brass shielding, since Fe, Cu, and Zn are in the region of Ni in the periodic table and would be expected to emit similar neutron spectra. The curve is a smooth fit to the spectrum, and it is extrapolated below 1.75 Mev by use of the Ni spectrum as a guide. The meager results on the background actually observed below 1.75 Mev are in agreement with this extrapolation. The background is a compilation of the results from each exposure. When the results from different exposures were combined, they were weighted according to the product of the beam through the target and the volume of emulsion scanned, which is consistent with the results from each exposure. In Fig. 7 the yield of background has been normalized to represent the number of background recoils in a 20^{o} cone per 10^{-3} cm^{3} of emulsion per 10^{14} particles through the target per 0.25 Mev energy interval. The background subtraction is made by the use of Figs. 6 and 7. The background correction

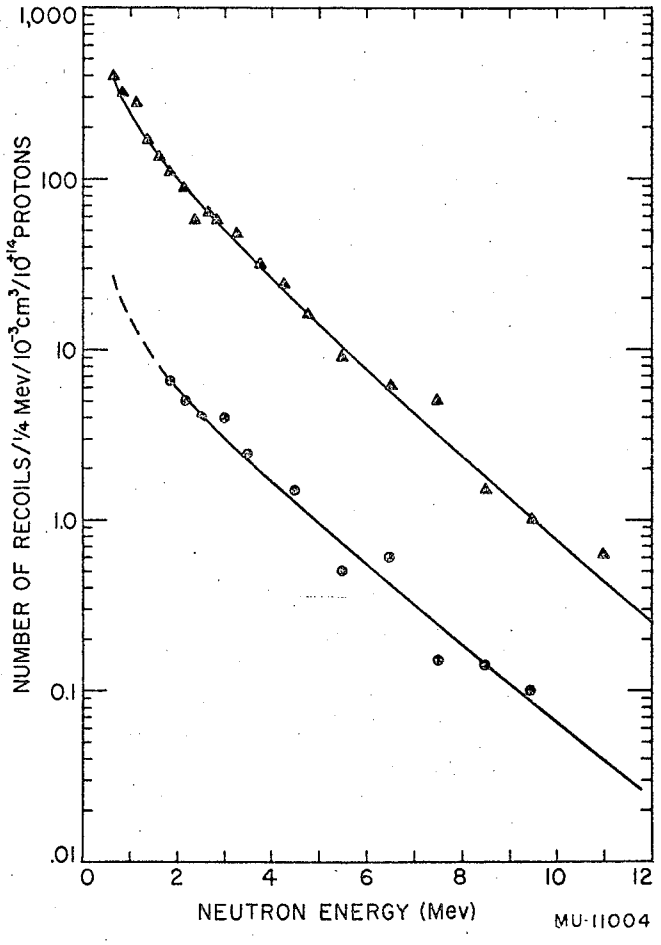

Fig. 7. The number of proton recoils as a function of neutron energy. The circles represent the combined spectrum of proton recoils observed in a backward 20° cone per 1/4 Mev neutron energy per 10^{-3} cm^3 of emulsion scanned per 10^{14} particles through the target. The triangles represent the spectrum of proton recoils observed in a forward 20° cone at 90° to a Ni target (arbitrary units). The similarity in shape to the spectrum from Ni is invoked to extend the background spectrum below 1.75 Mev.

Although the elastically scattered neutrons suffer no energy loss, they enter the emulsion surface at other than grazing angles and thus produce lower-energy recoils than the primary flux at the same neutron energy. With these considerations it is found that elastic scattering from the brass contributes 8% to the proton recoils at 1 Mev and slowly decreases to 2% at 15 Mev. Further details may be found in Appendix 4.

E. Correction for Absorption in the Target

The correction for the absorption of neutrons in the target was made by using the nonelastic cross sections published by Taylor et al.[36] These cross sections were further enhanced by the cross section for elastic neutron scattering for angles greater than 45^{o}.[34, 35] The absorption losses amounted to about 4% in the energy region 5 to 15 Mev and was somewhat less for energies less than 5 Mev. Absorption of neutrons in the cadmium light shield was negligible.

VI. RESULTS AND DISCUSSION

A. Energy Spectra

The corrected neutron energy spectra in the energy region 0.5 to 12.0 Mev observed from Au, Ag, Ni, Al, and C are presented in Figs. 8, 9, 10, 11, and 12. The errors shown are statistical errors only. The total number of events in a single spectrum is about 750. The absolute differential cross section scale has a further root-mean-square uncertainty of 18%. The cross-section scale for one element relative to another element is good to within 14%, because three of the activities used to determine the beam through a target are common to all bombardments (see Eq. (4)).

A common feature of all these spectra is the rapid rise in the differential cross section as the neutron energy decreases. None of the spectra shows a "peak," which presumably would appear if the energy spectrum could be obtained down to zero neutron energy.

Weisskopf[6] has derived an expression for the energy of neutrons emitted from excited nuclei, assuming that the excitation energy was distributed in a statistical manner among the nucleons within a nucleus. The emission of nucleons is then similar to the evaporation of molecules from a liquid. The energy spectrum of neutrons emitted from nuclei excited to the temperature T has the form

$$N(E_n)\, dE_n \sim \sigma_c(E_n)\, E_n\, e^{-E_n/T}\, dE_n, \qquad (13)$$

where E_n is the energy of the emitted neutron and $\sigma_c(E_n)$ is the capture cross section for the inverse reaction. The temperature T is a function of the excitation energy U. The theoretical dependence of the temperature on the excitation energy depends upon the particular nuclear model chosen (i.e. Fermi gas model or liquid drop model). According to Eq. (13), $\ln\left[\dfrac{d\sigma}{d\Omega dE/E_n\sigma_c}\right]$ plotted against E_n should be a straight line with the slope $-1/T$ if the observed neutrons come from nuclei with the same excitation energy. Figures 13 though 17 present the data as a "temperature" plot. The values of the inverse

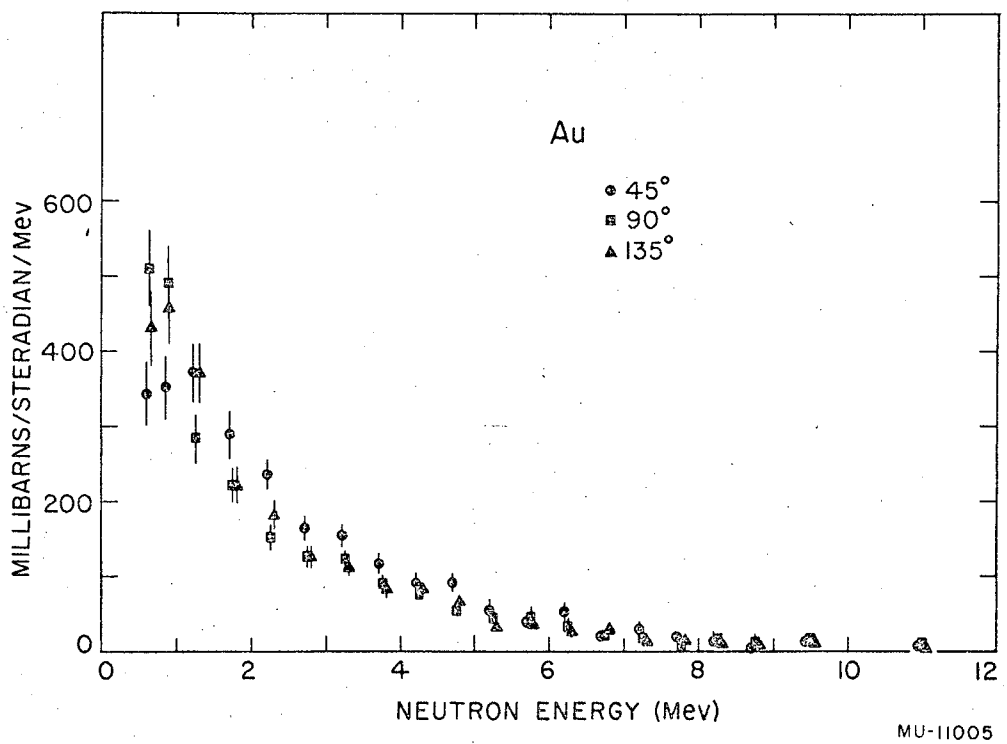

Fig. 8. Differential cross section for the production of neutrons from 190-Mev proton bombardment of gold.

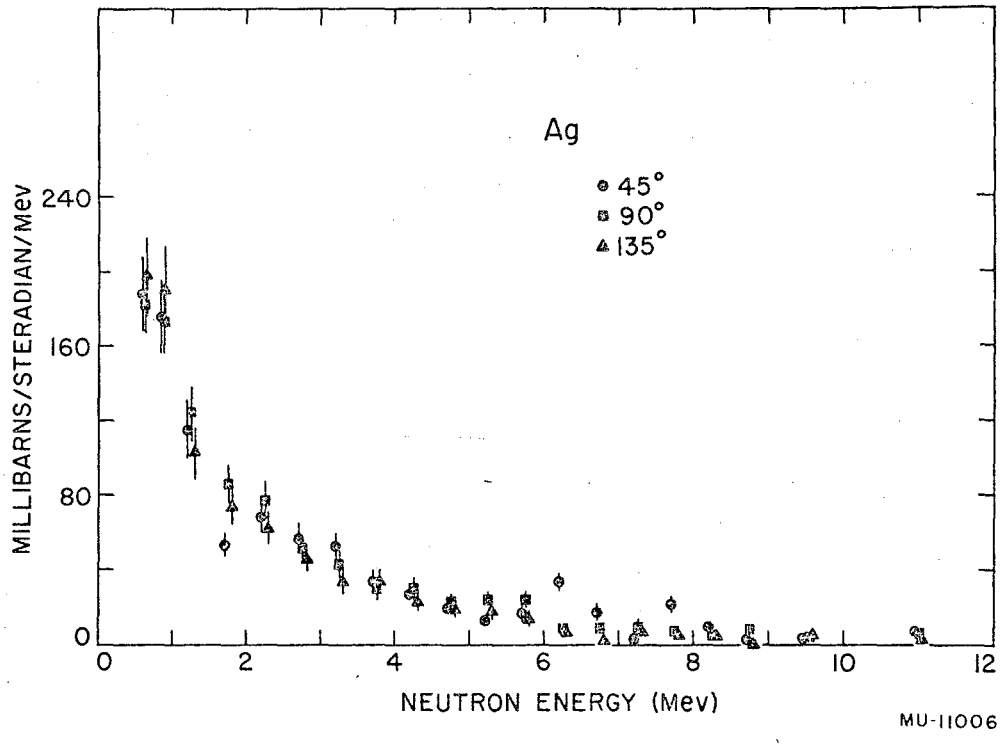

Fig. 9. Differential cross section for the production of neutrons from 190-Mev proton bombardment of silver.

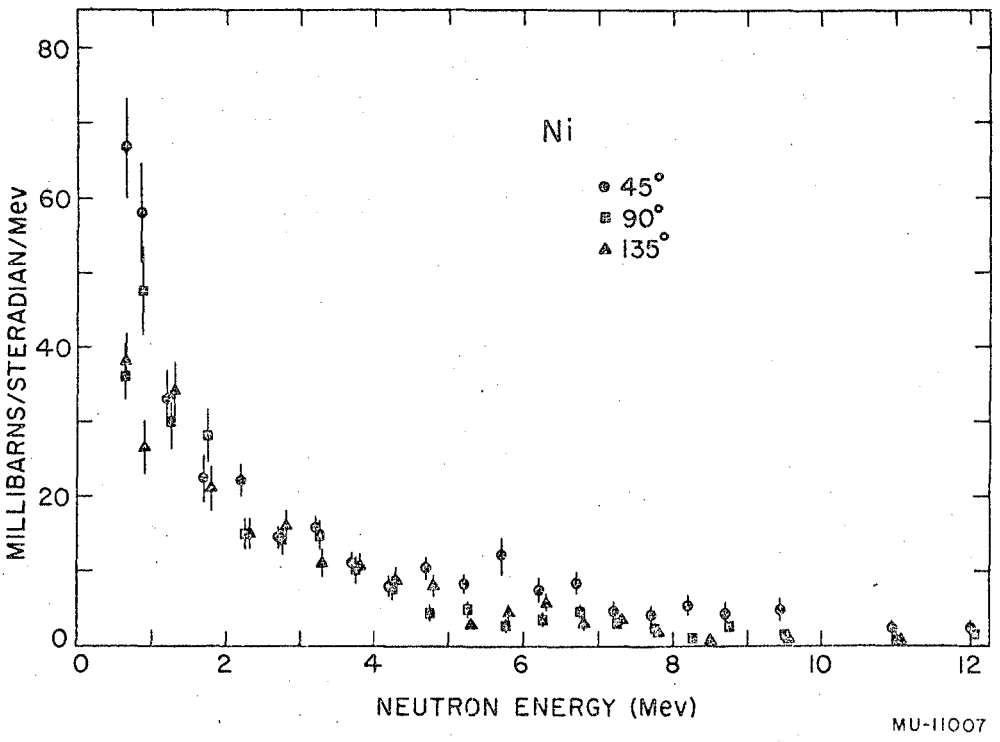

Fig. 10. Differential cross section for the production of neutrons from 190-Mev proton bombardment of nickel.

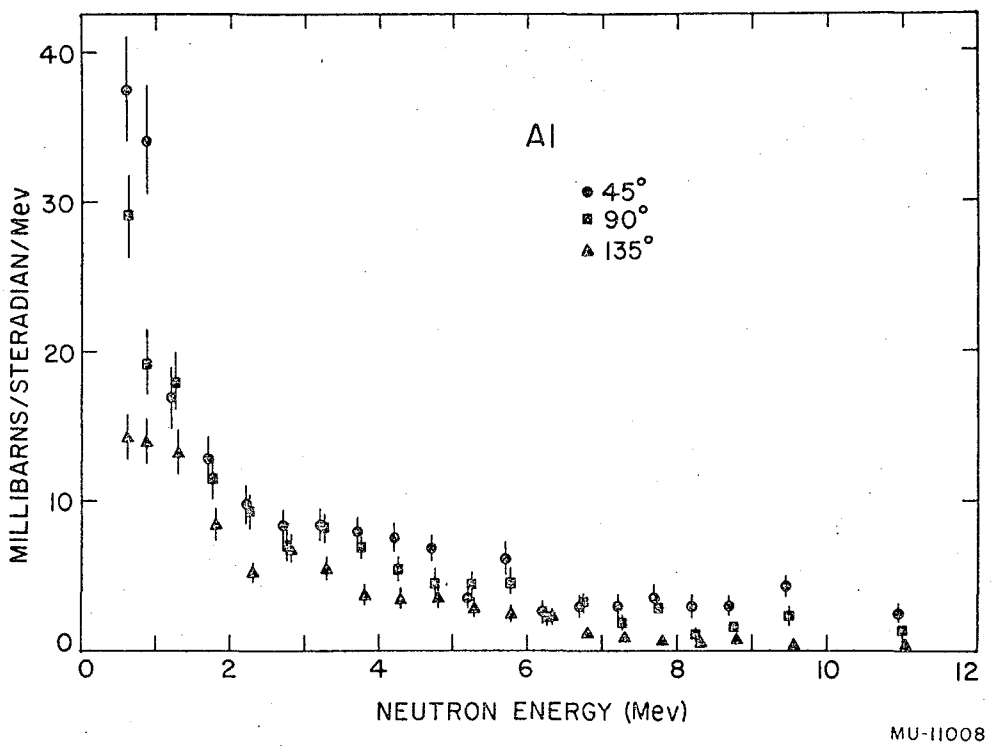

Fig. 11. Differential cross section for the production of neutrons from 190-Mev proton bombardment of aluminum.

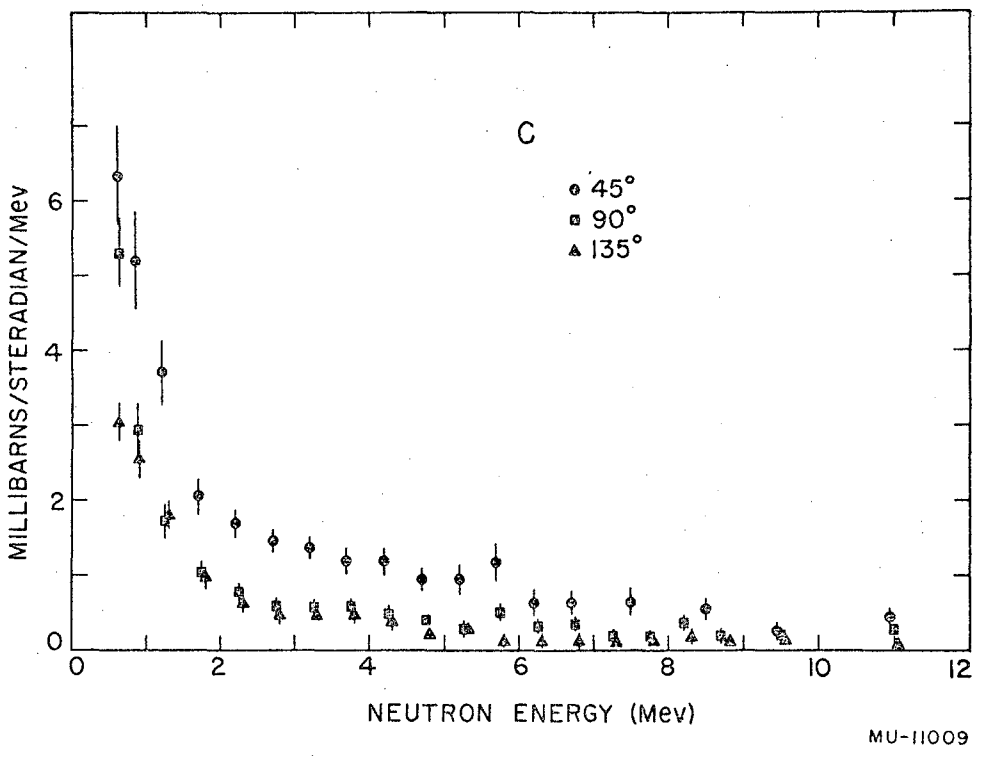

Fig. 12. Differential cross section for the production of neutrons from 190-Mev proton bombardment of carbon

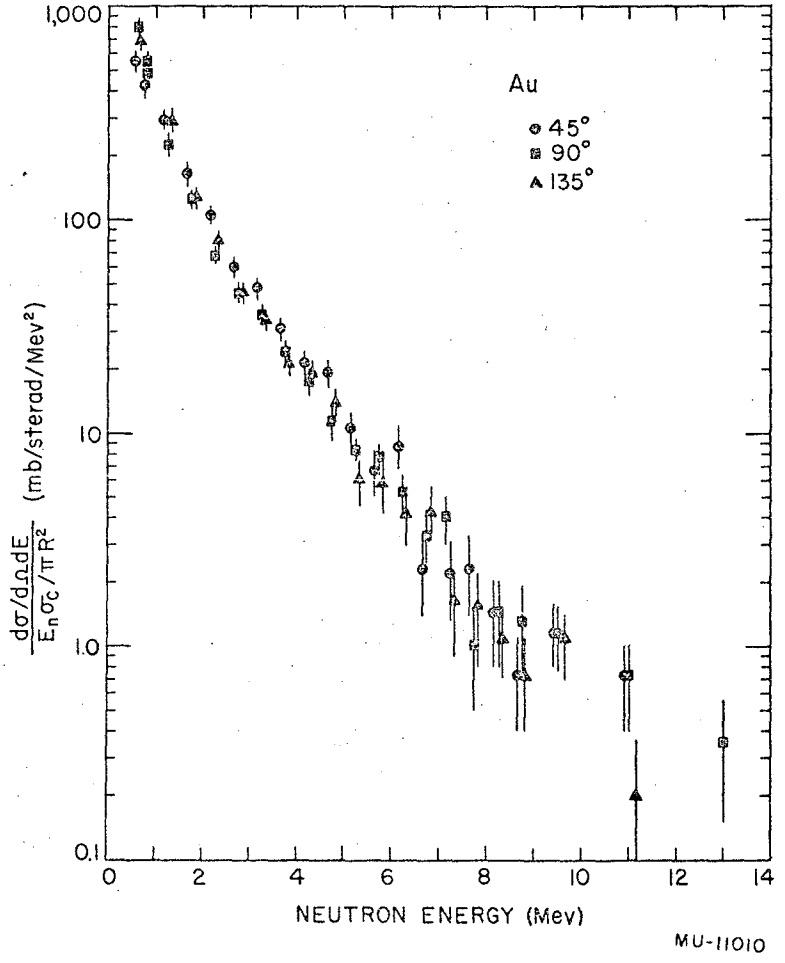

Fig. 13. $\ln \frac{d\sigma/d\Omega dE}{E_n \sigma_c/\pi R^2}$ versus neutron energy for Au.

Here σ_c is the neutron capture cross section for the inverse reaction; R is the nuclear radius of the target and was taken to be $1.5 \times 10^{-13} A^{1/3}$ cm. The values of $\sigma_c/\pi R^2$ were taken from Blatt and Weisskopf.[37] The errors shown are statistical errors only.

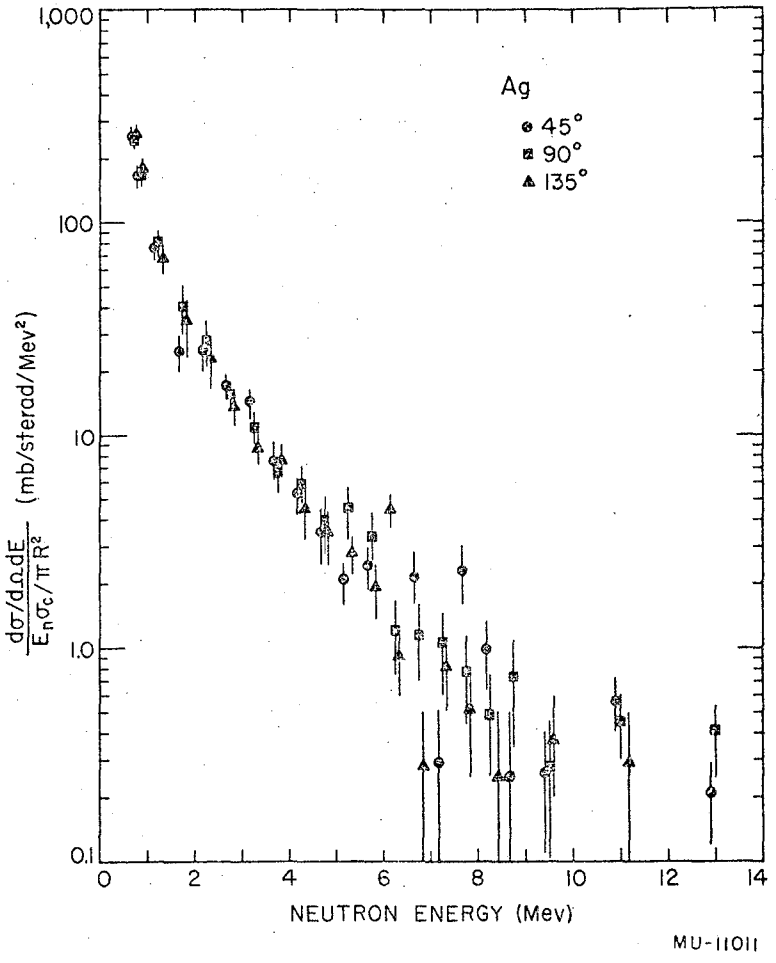

Fig. 14. $\ln \dfrac{d\sigma/d\Omega dE}{E_n \sigma_c/\pi R^2}$ versus neutron energy for Ag

Here σ_c is the neutron capture cross section for the inverse reaction; R is the nuclear radius of the target and was taken to be $1.5 \times 10^{-13} A^{1/3}$ cm. The values of $\sigma_c/\pi R^2$ were taken from Blatt and Weisskopf.[37] The errors shown are statistical errors only.

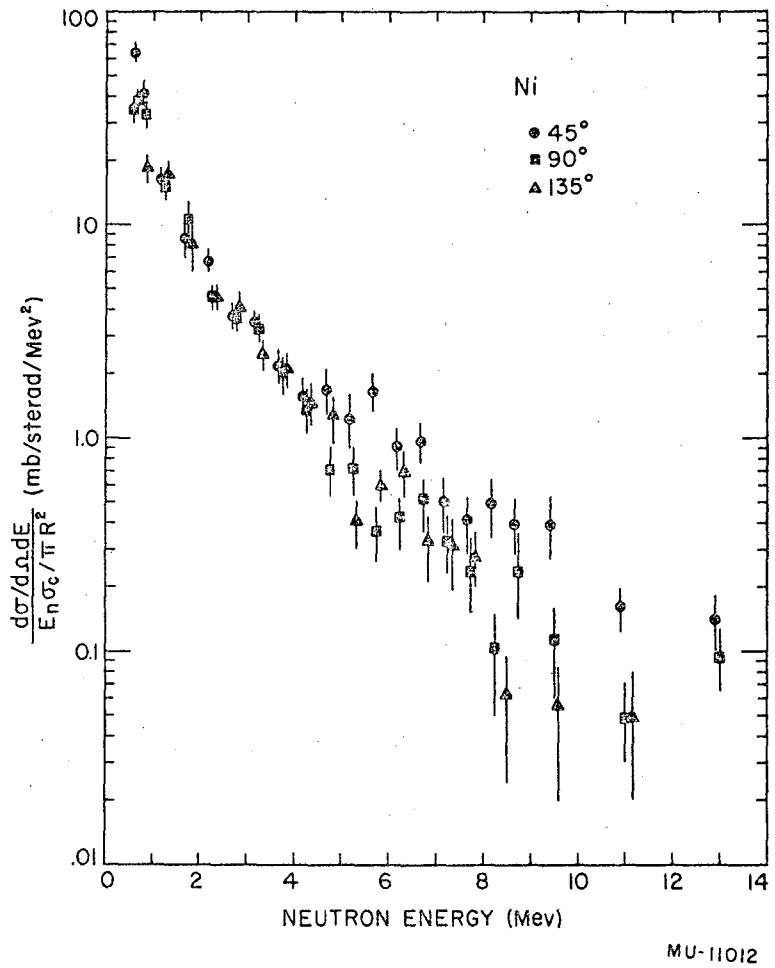

Fig. 15. $\ln \frac{d\sigma/d\Omega dE}{E_n \sigma_c/\pi R^2}$ versus neutron energy for Ni

Here σ_c is the neutron capture cross section for the inverse reaction; R is the nuclear radius of the target and was taken to be $1.5 \times 10^{-13} A^{1/3}$ cm. The values of $\sigma_c/\pi R^2$ were taken from Blatt and Weisskopf.[37] The errors shown are statistical errors only.

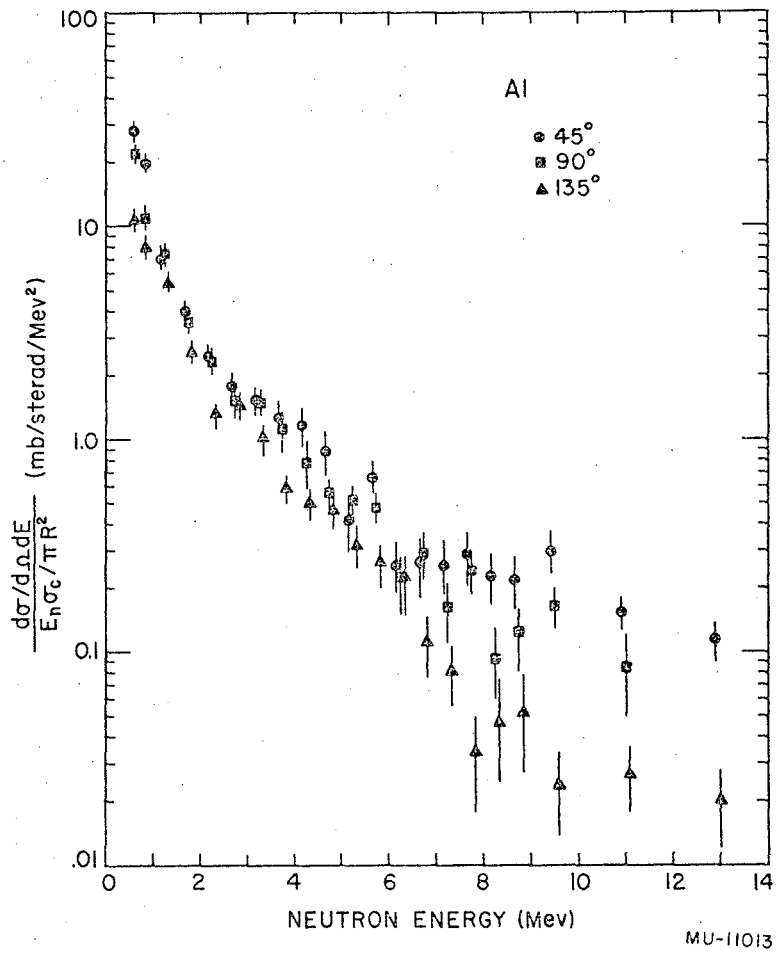

Fig. 16. $\ln \dfrac{d\sigma/d\Omega dE}{E_n \sigma_c/\pi R^2}$ versus neutron energy for A

Here σ_c is the neutron capture cross section for the inverse reaction; R is the nuclear radius of the target and was taken to be $1.5 \times 10^{-13} A^{1/3}$ cm. The values of $\sigma_c/\pi R^2$ were taken from Blatt and Weisskopf.[37] The errors shown are statistical errors only.

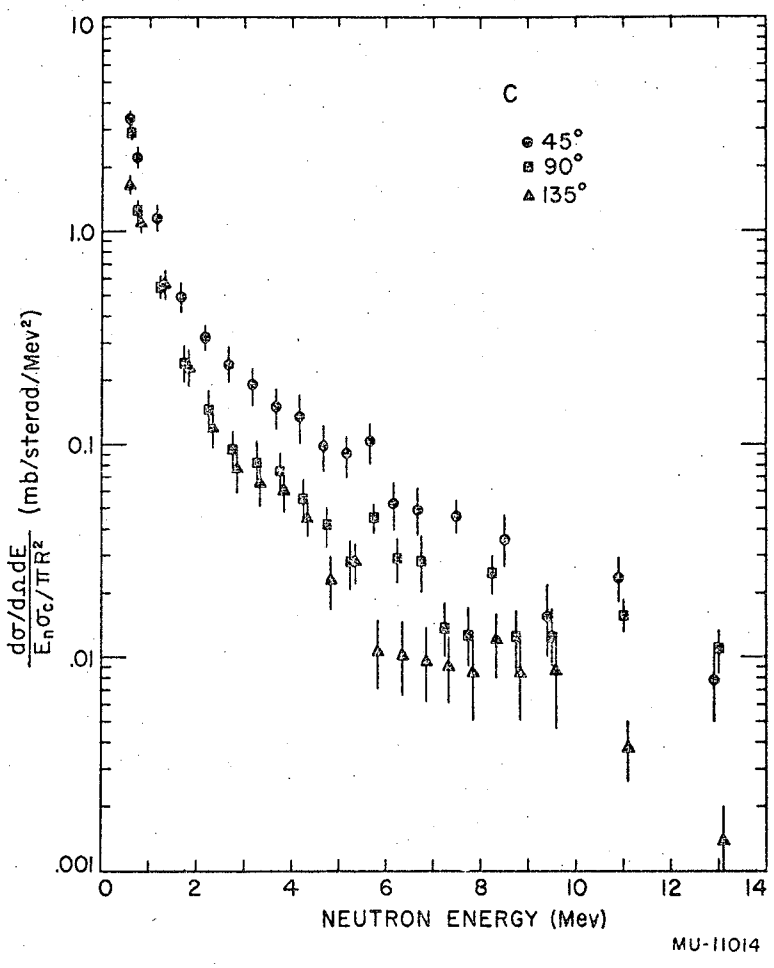

Fig. 17. $\ln \dfrac{d\sigma/d\Omega dE}{E_n \sigma_c/\pi R^2}$ versus neutron energy for ^{12}C.

Here σ_c is the neutron capture cross section for the inverse reaction; R is the nuclear radius of the target and was taken to be $1.5 \times 10^{-13} A^{1/3}$ cm. The values of $\sigma_c/\pi R^2$ were taken from Blatt and Weisskopf.[37] The errors shown are statistical errors only.

capture cross section, $\sigma_c(E_n)$, were taken from Blatt and Weisskopf.[37] Below 2 Mev all the curves have about the same slope, $T = 0.7 \pm 0.1$ Mev. Above 2 Mev, the data at different angles are consistent with different straight lines. The temperatures representing the data above 2 Mev are plotted against mass number in Fig. 18 together with corresponding temperatures resulting from 14-Mev neutron bombardment.[17]

It should be noted that the nuclei emitting the neutrons observed in this experiment must have a wide distribution of excitation energies resulting from the 190-Mev proton bombardment.[5] Furthermore, at this bombarding energy, there is a high probability of the emission of more than one neutron from a bombarded nucleus. The emitting nuclei are therefore expected to have a variety of temperatures to begin with and to go through a series of lower temperatures while evaporating particles. One would therefore expect the temperature plot to be a smooth curve, concave upwards. LeCouteur[38] presents formulae for the energy spectra of evaporated neutrons which take into account the cooling-down process due to the successive evaporation of particles. These formulae do not take into account the initial spread of excitation energies that result from 190-Mev proton bombardment. LeCouteur assumes that the excitation energy U is related to the temperature T by

$$U \sim T^{\delta}, \tag{14}$$

where δ is a constant that depends on a nuclear model. For the Fermi gas model $\delta = 2$. LeCouteur also treats the possibility of having $\delta = 3$. The energy spectrum of evaporated neutrons, when cooling is taken into account, is then given by

$$P(E)dE \sim E_n^{L-1} e^{-E_n/T} dE, \tag{15}$$

where $L = 16/11$ and $T^* = 11/12\ T_0$ for $\delta = 2$, and $L = 5/3$ and $T^* = 9/10\ T_0$ for $\delta = 3$. T_0 is the initial nuclear temperature. Plotting $\ln\left[\frac{d\sigma}{d\Omega dE}/E_n^{L-1}\right]$ against E_n should then result in a straight line with the slope $-1/T^*$. Figure 19 presents the data plotted in this way for $\delta = 2$. The data used in this plot were the average differential

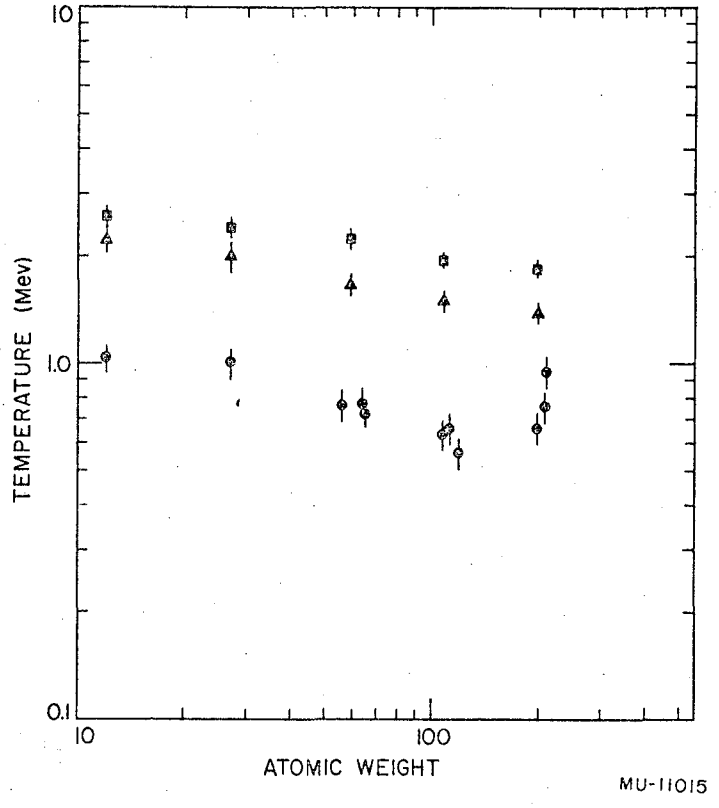

Fig. 18. The "temperature" obtained from neutron spectra as a function of atomic weight. The circles represent the values obtained by Graves and Rosen[17] at 14-Mev neutron bombardment. They used the definition $T = -\frac{d}{dE_n}\left\{\ln\left(\frac{d\sigma/d\Omega dE}{E_n}\right)\right\}$ for the temperature. The triangles represent my data for neutron energies greater than 2 Mev and are based on $T = -\frac{d}{dE_n}\left\{\ln\left(\frac{d\sigma/d\Omega dE}{\sigma_c E_n}\right)\right\}$ for the temperature. The squares represent my data for neutron energies greater than 2 Mev and are based on $T = -\frac{d}{dE_n}\left\{\ln\left(\frac{d\sigma/d\Omega dE}{E_n^{5/11}}\right)\right\}$ for the temperature.

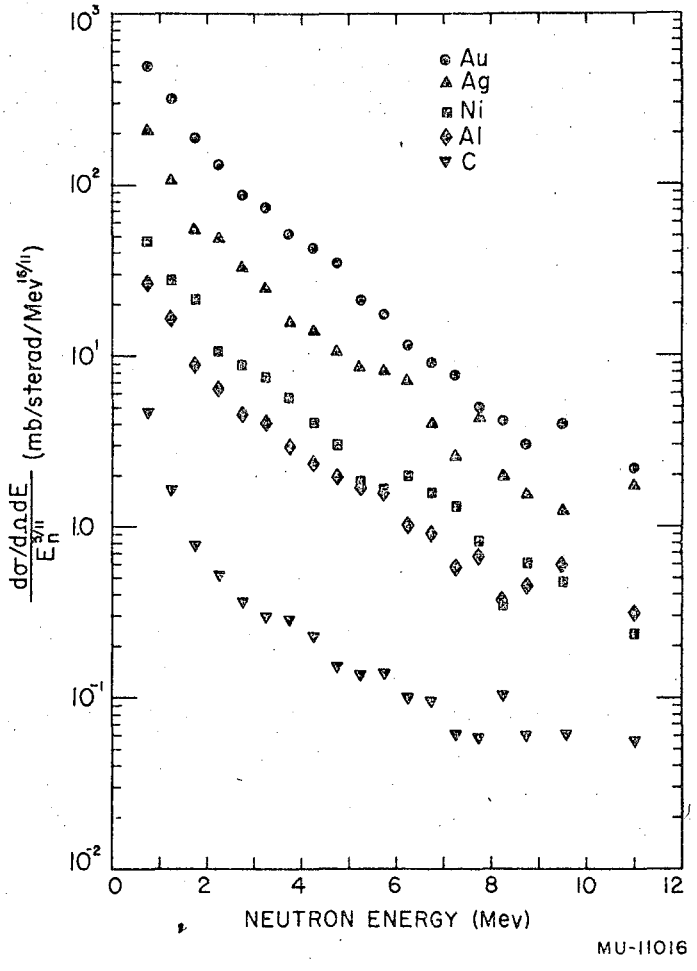

Fig. 19. Curve for $\ln \frac{d\sigma}{d\Omega dE/E_n^{5/11}}$ versus neutron energy for that part of the observed differential cross section which is consistent with isotropy in the center of mass of the emitting nucleus. The data should fall on a straight line if the cooling-down process could be described by $U \sim T^2$, where U is the excitation energy of the emitting nucleus at the nuclear temperature T. The statistical errors on the points are about the same as the statistical errors on the points in Figs. 13-17.

cross sections for Au and for Ag in the angular region 45° to 135° and the spherically symmetric part of the Ni, Al, and C data (the next section on angular distributions explains how these data were obtained). Figure 20 presents the same Au, Ag, and Ni data used in Fig. 19 but plotted for $\delta = 3$. The statistical errors of the points in Figs. 19 and 20 are about the same as the statistical errors of the points in Figs. 13-17. Equation (14) for $\delta = 2$ or $\delta = 3$ is seen to be in disagreement with the observed spectra, and this disagreement becomes worse as the atomic weight of the target is reduced. The temperatures obtained from Fig. 19, above a neutron energy of 2 Mev, are also plotted in Fig. 18.

B. Angular Distributions

The angular distribution of the low-energy neutrons from 190-Mev proton bombardment of Au and Ag appears to be isotropic in the angular region 45° to 135°. A definite angular variation begins to appear in the data from Ni. In going from 90° to 45° there is a noticeable increase in the yield of neutrons from Ni. In the results from Al there is an increase in neutron yield in going from 135° to 90° and a further increase in going from 90° to 45°. The angular variation observed with C is even more pronounced than it is with Al.

If the angular distributions of the neutrons between 0.5 Mev and 1.0 Mev are attributed to a center-of-mass velocity of the emitting nucleus, one can calculate this center-of-mass velocity by comparing the cross sections obtained at each angle (see Appendix 5). An average center-of-mass velocity of about $1.4 \times 10^{-2} c$ is required to explain the angular variation of the neutrons in the energy range 0.5 to 1.0 Mev from C, where c is the velocity of light. In Al, a center-of-mass velocity of about 1.2×10^{-2} c is required to explain the angular variation of these neutrons of the same energy, and the data from Ni demand a center-of-mass velocity of about $1.0 \times 10^{-2} c$. The angular variations of the neutrons from Ni, Al, and C above a neutron energy of 1 Mev cannot be explained by a single center-of-mass velocity. The 135° and 90° data, however, are consistant with a single average

center-of-mass velocity for the energies between 0.5 and about 3 Mev, and this center-of-mass velocity is the same as that required to fit the data at all three angles for the energies between 0.5 and 1.0 Mev. The center-of-mass velocity required to explain the angular variation observed between 90° and 45° for neutron energies greater than 1 Mev increases with the increasing neutron energy. Beyond about 3 Mev an apparent center-of-mass velocity would be required that would represent a momentum for the evaporating nucleus that is greater than the momentum of the bombarding proton. The center-of-mass velocities obtained by comparing the 135° and 90° data for neutron energies greater than 3 Mev have the same behavior as the velocities obtained by comparing the 90° and the 45° data above 1 Mev.

That the low-energy neutron data are consistent with an isotropic center-of-mass distribution for all bombarded targets, and that the resulting center-of-mass velocities decrease monotonically with increasing mass number of the target, is convincing evidence for the evaporation model for the production of these neutrons. However, the angular variations above a neutron energy of 1 Mev and the inability to explain these variations in terms of a center-of-mass motion is evidence for the presence of neutrons produced in the cascade process.

C. Absolute Yields

Presumably an isotropic center-of-mass differential cross section represents the yield of particles due to the evaporation process. As discussed in the previous section, the data are believed to indicate an isotropic center-of-mass distribution together with an angle-dependent yield attributed to the cascade process. To estimate the total yield of neutrons due to the evaporation process alone, an attempt was made to integrate only that part of the differential cross section which yielded an isotropic center-of-mass distribution. For the Au and Ag data, this amounted to simply averaging the laboratory data over angle. For the Ni, Al, and C data, the 90° data from 0.5 to 3.0 Mev and an average of the 90° and 135° data for neutron energies greater than 3 Mev was used as representative of the differential cross section (c.m.) due

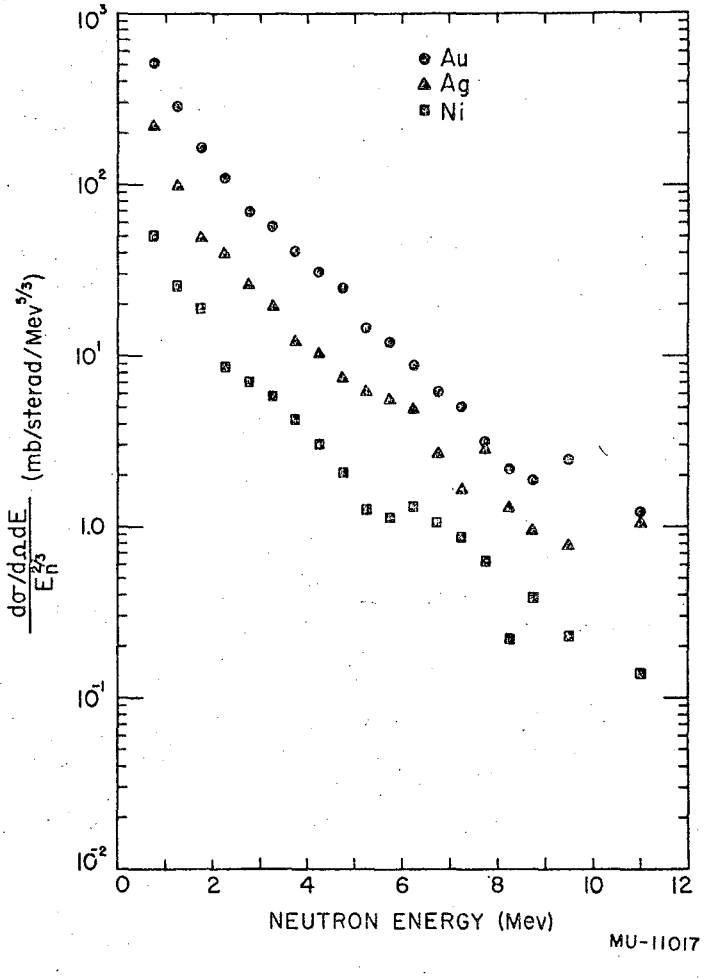

Fig. 20. Curve of $\ln \dfrac{d\sigma}{d\Omega dE/E_n^{2/3}}$ versus neutron energy for the same Au, Ag, and Ni data used in Fig. 19. The data should fall on a straight line if the cooling-down process could be described by $U \sim T^3$, where U is the excitation energy of the emitting nucleus at the nuclear temperature T.

to evaporation alone. The 90° and 135° data for $0.5 < E_n < 3$ Mev were found to be consistent with a single center-of-mass velocity (see Appendix 5), and it was argued that the 90° data are essentially unchanged in transforming from the center-of-mass to the laboratory system. Above 3 Mev the yield of cascade neutrons in the 90° data begins to be apparent. However, the 135° cross section is somewhat lower than it is in the center-of-mass system, so that an average of the 90° and 135° data above 3 Mev should somewhat cancel these two effects. The differential cross sections so obtained were integrated over energy up to 12 Mev for Au and Ag, 14 Mev for Ni, 16 Mev for Al, and 20 Mev for C. The differential cross sections were extended down to zero neutron energy by assuming that the "temperature" of about 0.7 Mev observed between 0.5 and 2 Mev held all the way down to zero energy. The differential cross sections integrated over energy were then integrated over angle by multiplying by 4π steradians. The resulting total cross sections are plotted in Fig. 19 together with the total neutron cross sections for the neutron energy interval 0.5- 12.0 Mev observed from 14-Mev neutron bombardment.[17] The statistical error in the total evaporation cross section is about 3%. The error introduced into the total evaporation cross section due to possible inclusion of cascade-produced neutrons is estimated to be about 5% for Ni, 10% for Al, and 15% for C. Possible cascade contamination was estimated by extrapolating to zero energy that part of the 90° data above 4 Mev that could not be explained by the angular variation expected from a center-of-mass motion. These errors are included in Fig. 21.

It is seen that the yield of low-energy neutrons increases with mass number more rapidly at 190-Mev proton bombardment than it does at 14-Mev neutron bombardment. At 190-Mev proton bombardment, light elements are more transparent than the heavier elements.[39] More excitation energy is therefore expected to be delivered to the heavy elements than to the light elements at this bombarding energy.[5] The higher excitation energy is expected to result in higher yields of evaporation products. The higher yield of neutrons from 14-Mev neutron

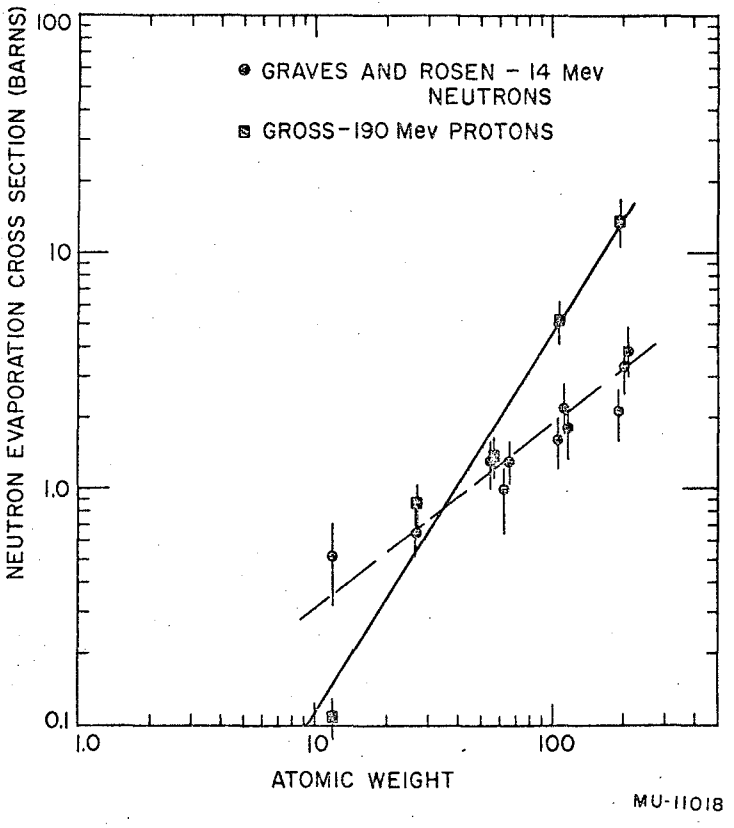

Fig. 21. Total cross section for the production of "evaporation" neutrons versus atomic weight for 190-Mev proton bombardment and 14-Mev neutron bombardment. The lines show the apparent trends of the data.

bombardment of mass numbers less than about 30, as compared to the yield resulting from 190-Mev proton bombardment, can probably be attributed to the use of neutrons rather than protons for the bombarding particles.

The observed increase in the yield of neutrons with increasing mass number is in general agreement with the spallation studies by the chemists.[40,41] The chemists examine the yield of end products resulting from high-energy bombardment of an element. They find a yield of neutron-deficient end products that increases with the mass number of the target.

The total neutron cross sections, observed in the manner outlined above, are tabulated in Table I. They are followed by the attenuation cross sections, σ_a, for 190-Mev protons in the target material. The average numbers of neutrons emitted per elastic collision, n_n, were obtained by dividing the total neutron cross section by the attenuation cross section; they are tabulated also. The average numbers of protons, n_p, and of alpha particles, n_α, have been obtained in similar manner by using the data from Bailey.[15] It should be emphasized that these numbers refer to the average number of particles emitted in the so-called evaporation energy region and do not include yields in the cascade energy region. The average neutron energies, E_n, given in the table were obtained from the observed energy spectra; the values obtained in this way may be too low by about 0.5 Mev for Al, and 1 Mev for C, because the average neutron energy is very sensitive to the high-energy neutron yield. For Al and C, the energy spectra probably have not been extended to high enough energy. The uncertainities quoted above were obtained by comparison with average neutron energies obtained from evaporation theory, which predicts that the average emitted neutron energy is twice the temperature.[6] The average proton energy, E_p, and average α-particle energy, E_α, in the evaporation energy region were obtained from the data of Bailey.[15] Errors in the number of neutrons, protons and α particles emitted in the evaporation process are estimated to be about 20%. This includes a 3% error in the attenuation cross sections for 190-Mev protons.[39]

Table I

The total neutron evaporation cross section σ_n; the attenuation cross section σ_a; the number of evaporation neutrons protons, and alpha particles per nuclear collision, n_n, n_p, and n_α; the average kinetic energy, E_n, E_p, E_α; and the average excitation energy U for the various 190-Mev proton bombardments.

Target	σ_n	σ_a	n_n	E_n (Mev)	n_p	E_p (Mev)	n_α	E_α (Mev)	U (Mev)
C	0.104 ± 0.026	0.23	0.45 ± 0.11	3.4	0.42 ± 0.10	4.4	0.55 ± 0.11	7.1	27 ± 5
Al	0.86 ± 0.17	0.41	2.1 ± 0.4	3.0	0.80 ± 0.16	6.1	0.42 ± 0.09	7.0	50 ± 8
Ni	1.38 ± 0.28	0.71	2.0 ± 0.4	2.7	1.10 ± 0.22	7.45	0.20 ± 0.04	12.0	57 ± 9
Ag	5.17 ± 1.03	1.10	4.7 ± 0.9	2.5	0.56 ± 0.11	9.8	0.18 ± 0.04	17.4	69 ± 12
Au	13.64 ± 2.7	1.70	8.0 ± 1.6	2.4	0[a]	..	0.10 ± 0.02	25.2	83 ± 17

[a] Au proton spectrum is interpreted as being entirely due to the cascade process.

From the results of Table I, one can estimate an excitation energy U for the evaporating nucleus. These appear in the last column of the table. The values for the excitation energy were arrived at by balancing mass and energy as follows:

Let $M(A_0, Z_0)$ be the mass of a target whose mass number is A_0 and atomic number Z_0. All masses are to be in Mev units. In a collision, n_{cp} cascade protons and n_{cn} cascade neutrons are knocked out of the target and we are left with a nucleus of ground-state mass $M(A_c, Z_c) = M(A_0 - n_{cp} - n_{cn}, Z_0 - n_{cp})$ and with excitation energy U. This nucleus then evaporates n_{ei} particles of mass m_i and kinetic energy E_i until a nucleus of ground-state mass $M(A_e, Z_e) = M(A_c - \sum_i n_{ei} m_i, Z - \sum_i Z_{ei})$ is reached with excitation energy U_e. Balancing mass and energy, we have

$$M(A_c, Z_c) + U = \sum_i n_{ei}(m_i + E_i) + M(A_e, Z_e) + U_e . \qquad (16)$$

It is estimated by McManus and Sharp[5] that roughly one proton and one neutron appear in the cascade for the elements between Al and U. Assuming that one proton and neutron are removed by the cascade process, one can calculate the mass $M(A_c, Z_c)$ by using the semiempirical mass formula due to Fermi.[42] Using the values obtained for the average number of particles removed in the evaporation process, one can again use the semiempirical mass formula to obtain the average ground-state mass of the nucleus that ends the evaporation stage, $M(A_e, Z_e)$. The average excitation energy remaining in $M(A_e, Z_e)$ has been taken to be one-half the binding energy of the easiest nucleon to remove from $M(A_e, Z_e)$. This binding energy can also be calculated from the semiempirical mass formula. In application of the semiempirical formula, odd-even effects were neglected because average masses were desired. For C the method using the semiempirical mass formula breaks down, and the excitation energy was estimated by assuming an average binding energy of 10 Mev per neutron, 10 Mev per proton, and 8 Mev per α particle emitted in the evaporation stage.[43] Each particle takes away an energy equal to its average binding energy

plus its average kinetic energy. An estimated 7 Mev in excitation energy of the residual nucleus was added so as to obtain the total excitation energy for the C bombardment.[43]

The excitation energies so obtained were plotted against atomic weight of the target in Fig. 22. The errors in the excitation energies were estimated by using the semiempirical mass formula together with the errors in the numbers of neutrons, protons, and α particles emitted under the same bombardment conditions.[15] The errors in the numbers of protons and α particles emitted are not entirely independent of the number of neutrons emitted since a common beam-monitoring method was used to obtain these results. Three of the activities used to estimate the beam through a target (see Eq. 4) were common to Bailey's experiment and this experiment. The average number of neutrons and the average number of protons emitted by a target may therefore be systematically too high or too low by about 14%. The average number of protons and the average number of α particles emitted by a target may be systematically too high or too low by about 18%, because the yields of protons and α particles depend upon the same beam estimate. These systematic errors have been included in the total estimated error for the excitation energy. The relative error in the excitation energy between one element and another is about 14%.

Figure 22 also presents the theoretical estimate of McManus and Sharp,[5] who used the Monte Carlo method[3] to calculate the excitation energies resulting from various bombardments of Al, Ag-Br, and U. The theoretical estimate lies somewhat below the experimental estimate presented here. The experimental points for Ni, Al, and C might contain further systematic errors of 5%, 10%, and 15% respectively due to inclusion of cascade-produced particles in the evaporation energy region. However, systematic errors of this magnitude would not bring into agreement the theoretical and experimental results. On the other hand, the theoretical estimate of the excitation energy may be low for two reasons: (a) reflection of particles at the nuclear surface was neglected, and (b) nucleons in the nucleus were characterized by a Fermi momentum distribution, whereas a Gaussian momentum distribution containing higher-energy components would be more in agreement with experimental results.[44]

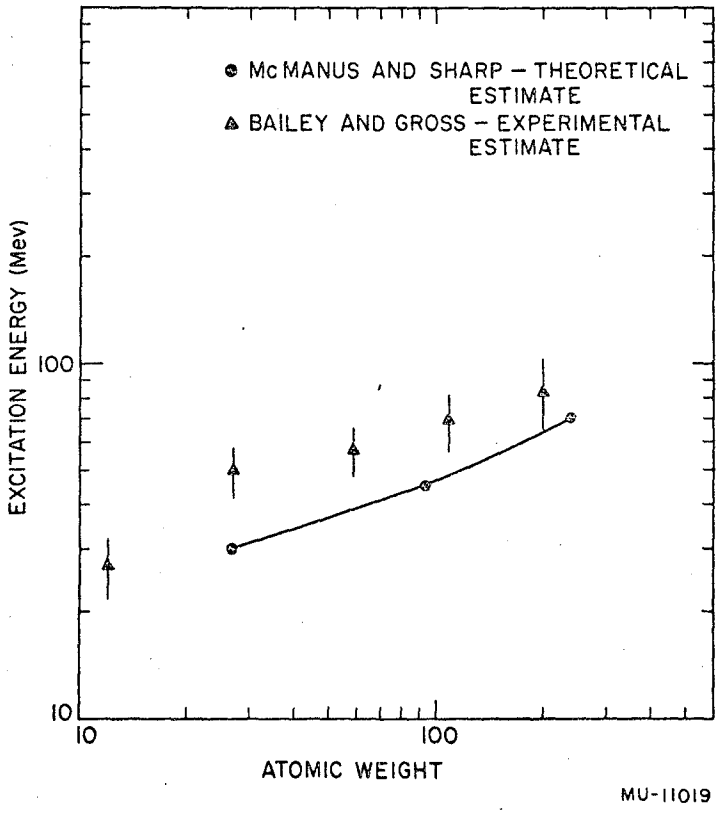

Fig. 22. The average excitation energy of the residual nucleus as a function of atomic weight of the target for 190-Mev proton bombardment.

For comparison purposes, the yield of low-energy neutrons from 150-Mev proton bombardment of W, Ag, Cu, and Al obtained by Skyrme and Williams are presented in Table II.[18,45] These results have been obtained by observing proton recoils in nuclear emulsions at 180° to the proton beam. The neutrons traveled 18.9 meters in air before being detected and thus in contrast to my experiment the neutron yield had to be corrected appreciably for attenuation in this air path. To obtain the total neutron yield, Skyrme and Williams assumed that the angular distribution of neutrons was isotropic in the laboratory system. Considering the difference in bombarding energy between my experiment and the experiment of Skyrme and Williams, the results on the yields of evaporation neutrons are in fair agreement except for the Al target. The disagreement in the yield of neutrons from Al is undoubtedly due to their assumption of an isotropic angular distribution in the laboratory system.

Table II

Average number of protons emitted in the evaporation energy region as a result of 150-Mev proton bombardment of various elements

Element	Al	Cu	Ag	W
n_n	0.6	1.6	4.0	4.9

ACKNOWLEDGMENTS

I am indebted to Dr. Walter H. Barkas for his help and guidance throughout the course of this research. I am grateful to Dr. Robert Thornton for his interest and encouragement. To Mr. L. Evan Bailey I am indebted for generous assistance and for many illuminating discussions.

The machine calculations were supervised by Mr. James Baker. Much of the scanning and many hand calculations were performed by Mrs. Toni Woodford. Mrs. Mary Ann Gross helped in the preparation of this manuscript as well as with many of the calculations.

I also wish to thank Mr. James Vale and the members of the cyclotron crew for their help in making the bombardments.

This work was done under the auspices of the U.S. Atomic Energy Commission.

APPENDIX

1. The Error in the Solid-Angle Factor, $f(\theta_M)$

According to Eq. (6), the fractional error in the solid-angle factor $f(\theta_M)$, is given by

$$\frac{\delta f(\theta_M)}{f(\theta_M)} = \frac{\delta(\cos 2\theta_M)}{(1-\cos 2\theta_M)} = 4.27\,\delta(\cos 2\theta_M), \text{ for } \theta_M = 20^\circ \quad (17)$$

Notice that $\frac{\delta f(\theta_M)}{f(\theta_M)}$ is four times as large for $\theta_M = 10^\circ$ as it is for $\theta_M = 20^\circ$. A larger cone therefore allows a more accurate determination of absolute yields. However, the energy resolution suffers as the cone angle increases.

$\cos 2\theta_M$ may be put in terms of the dip angle β and the projected angle α by use of Eq. (7):

$$\cos 2\theta_M = 2\cos^2\theta_M - 1 = 2\cos^2\alpha\cos^2\beta - 1. \quad (18)$$

Assuming that the errors in α and β are independent, we have the error in $\cos 2\theta_M$ given by

$$\delta(\cos 2\theta_M) = 2\left\{\cos^4\alpha\left[\delta(\cos^2\beta)\right]^2 + \cos^4\beta\left[\delta(\cos^2\alpha)\right]^2\right\}^{1/2}. \quad (19)$$

According to Eq. (8), $\cos^2\beta$ is given by

$$\cos^2\beta = \frac{1}{1+\tan^2\beta} = \frac{1}{1+\left(\frac{s\Delta z}{kr_H}\right)^2} \approx 1 - \left(\frac{s\Delta z}{kr_H}\right)^2, \text{ for } \beta \text{ small}, \quad (20)$$

where s, Δz, k, and r_H are as defined in Eq. (8).

By far the largest uncertainty in $\cos\beta$ is due to the uncertainty in the dip of the track, Δz. The uncertainty in $\cos^2\beta$ is then

$$\delta(\cos^2\beta) \approx 2(s/kr_H)^2\,\Delta z\,\delta(\Delta z). \quad (21)$$

For the emulsions used in this experiment $s = 2.17$. The standard deviation of Δz was found, from repeated measurements on the same tracks, to be about 0.25 micron. The average dip angle β for the conditions $\theta_M = 20^\circ$ is about 12°. This determines the average dip Δz for the same condition. Equation (21) then yields the following uncertainties for $\cos^2 \beta$:

$$\delta(\cos^2\beta) = \begin{cases} 1 \times 10^{-2} \text{ for } kr_H = 22\mu, & (1.25 \text{ Mev}), \\ 2 \times 10^{-2} \text{ for } kr_H = 11\mu, & (0.75\text{-}1 \text{ Mev}), \\ 3 \times 10^{-2} \text{ for } kr_H = 7.5\mu, & (0.5\text{-}0.75 \text{ Mev}). \end{cases} \tag{21'}$$

The uncertainty in $\cos^2 \alpha$ is given by

$$\delta(\cos^2 \alpha) = -2 \cos \alpha \sin \alpha \, \delta\alpha \, . \tag{22}$$

The uncertainty in projected angle $\delta\alpha$ varies for the length of track measured. This error is about 0.3° for ranges greater than 10 microns and about 0.5° for tracks less than 10μ. The average value of α, for the condition $\theta_M = 20^\circ$, is about 12°. The average uncertainty in $\cos^2 \alpha$ is then

$$\overline{\delta(\cos^2 \alpha} = \begin{cases} 2.1 \times 10^{-3} \text{ for } kr_H > 10 \text{ microns} \\ 3.5 \times 10^{-3} \text{ for } kr_H < 10 \text{ microns} \end{cases} \tag{22'}$$

The values of $\delta(\cos^2 \beta)$ and $\delta(\cos^2 \alpha)$ from Eq. (21') and (22') may then be used to obtain $\delta(\cos 2\theta_M)$ from Eq. (19). The resulting values for $\delta(\cos 2\theta_M)$, substituted into Eq. (17), give the following results:

$$\frac{\delta f(20^\circ, E_n)}{f(20^\circ, E_n)} = \begin{cases} 8\%, & E_n > 1 \text{ Mev}, \\ 17\%, & 0.75 \text{ to } 1 \text{ Mev}, \\ 25\%, & 0.5 \text{ to } 0.75 \text{ Mev}. \end{cases} \tag{17'}$$

These are the fractional errors in $f(20^\circ, E_n)$ expected from a single measurement. Aside from the variations of events with space angle (Eq. (5)), one would expect that the number of tracks actually

lying outside a cone but measured as lying inside the cone should equal the number of tracks that actually lie inside the cone but which are measured as outside the cone.

2. Uncertainty in the Energy Interval, ΔE_n

The fractional error in the neutron energy may be obtained from Eq. (10):

$$\frac{\delta E_n}{E_n} = \left[\left(\frac{\delta E_p}{E_p}\right)^2 + \left(\frac{\delta(\cos^2\theta)}{\cos^2\theta}\right)^2\right]^{1/2} . \tag{23}$$

The error in $\cos^2\theta$ may be put into terms of the error in $\cos 2\theta$ (the latter is evaluated in Appendix 1):

$$\frac{\delta(\cos^2\theta)}{\cos^2\theta} = \frac{\delta \cos 2\theta}{1 + \cos 2\theta} \approx 1/2\ \delta(\cos 2\theta), \text{ for } \theta \text{ small.} \tag{24}$$

From the error in $\cos 2\theta$ obtained in Appendix 1, we get

$$\frac{\delta(\cos^2\theta)}{\cos^2\theta} = \begin{cases} 1.5\%, & E_n > 1 \text{ Mev}, \\ 2.5\%, & 0.75 < E_n < 1 \text{ Mev}, \\ 3\%, & 0.5 < E_n < 0.75 \text{ Mev}. \end{cases} \tag{24'}$$

The error in the proton energy may be estimated from the range-energy relation. In a small energy interval the range-energy relation[26] may be represented by

$$E_p = \left[\frac{R_p}{K(E_p)}\right]^{3/2} = \left[\frac{R_H}{K(E_p)\cos\beta}\right]^{1/2} , \tag{25}$$

where $K(E_p)$ is a slowly varying function of proton energy. The fractional error in E_p is then

$$\frac{\delta E_p}{E_p} = \frac{2}{3}\left[\frac{\delta R_H}{R_H}^2 + \frac{1}{4}\ \frac{\delta(\cos^2\beta)}{\cos\beta}^2\right]^{1/2} \tag{26}$$

The quantity R_H is estimated to be about 0.3μ. The fractional error in R_H is then

$$\frac{\delta R_H}{R_H} = \begin{cases} 0.05, & 0.5 < E_n < 0.75 \text{ Mev}, \\ 0.03, & 0.75 < E_n < 1 \text{ Mev}, \\ 0.025, & 1 < E_n < 1.25 \text{ Mev}. \end{cases} \tag{27}$$

The uncertainty in $\cos^2 \beta$ is given in Eq. (21') of Appendix 1. Insertion of the results of Eqs. (21') and (27) into Eq. (26) gives

$$\frac{\delta E_p}{E_p} = \begin{cases} 0.010, & E_n > 1 \text{ Mev}, \\ 0.022, & 0.75 < E_n < 1 \text{ Mev}, \\ 0.035, & 0.5 < E_n < 0.75 \text{ Mev}. \end{cases} \tag{26'}$$

Combining the results of Eqs. (24') and (26') with Eq. (23) gives

$$\frac{\delta E_n}{E_n} = \begin{matrix} 0.02, & E_n > 1 \text{ Mev}, \\ 0.03, & 0.75 < E_n < 1 \text{ Mev}, \\ 0.045, & 0.5 < E_n < 0.75 \text{ Mev}. \end{matrix} \tag{23'}$$

The error in the energy interval ΔE_n should then be

$$\frac{\delta(\Delta E_n)}{\Delta E_n} = \sqrt{2}\,\frac{\delta E_n}{E_n} = \begin{cases} 0.03, & E_n > 1 \text{ Mev}, \\ 0.04, & 0.75 < E_n < 1 \text{ Mev}, \\ 0.065, & 0.5 < E_n < 0.75 \text{ Mev}. \end{cases} \tag{28}$$

This is the fractional error in ΔE_n expected from a single measurement. When a large number of events are measured about as many events are "scattered" into the energy interval ΔE_n as are "scattered" out of the energy interval ΔE_n.

3. Correction for Exit

The number of proton recoils in a 20° cone per neutron energy interval must be corrected for the probability that some of these recoils may leave the emulsion, whose thickness is t.

Consider recoils of range R originating in an element of emulsion thickness dy which is located a distance y from one emulsion surface and a distance $t-y$ from the other emulsion surface (see Fig. 23). Let the z direction be the neutron direction, then the emulsion surfaces are parallel to the x-y plane. Let the track be produced into the element of space angle between θ and $\theta+d\theta$ and have an azimuthal angle between ϕ and $\phi+d\phi$. If the production of recoils throughout the emulsion volume is assumed to be random, then the fraction of recoils produced in dy is just dy/t. The fraction of recoils produced between θ and $\theta+d\theta$ is given by Eq. (5) to be $N_0(E_n) \sin z\,\theta\, d\,\theta$, where $N_0(E_n)$ is the total number of recoils produced by neutrons of energy E_n. Assuming a random production of recoils in azimuthal angle, we have the fraction of recoils between ϕ and $\phi+d\phi$ equal to $d\phi/2\pi$. Therefore the number of recoils produced between y and $y+dy$, θ and $\theta+d\theta$, and ϕ and $\phi+d\phi$ is

$$N(y, \theta, \phi)\, dyd\theta d\phi = N_0(E_n) \sin 2\theta \frac{dy}{t} \frac{d\phi}{2\pi} \qquad (29)$$

Consider those tracks that are traveling toward the top emulsion surface (Fig. 23), and assume that their range R is rectilinear. If $R \sin \theta > y$, then those tracks for which $R \sin\theta \cos\phi > y$ leave the emulsion. The number of tracks that leave the top emulsion surface under these conditions is

$$\Delta N_{top}\, dyd\theta = N_0(E_n) \sin 2\theta d\theta \frac{dy}{t} \int_{-\cos^{-1}(y/R \sin\theta)}^{\cos^{-1}(y/R \sin\theta)} \frac{d\phi}{\pi}$$

$$= \frac{N_0(E_n)}{\pi t} \sin 2\theta\, d\theta\, dy \cos^{-1}(y/R \sin\theta),$$

$$\text{for } R \sin\theta > y. \qquad (30)$$

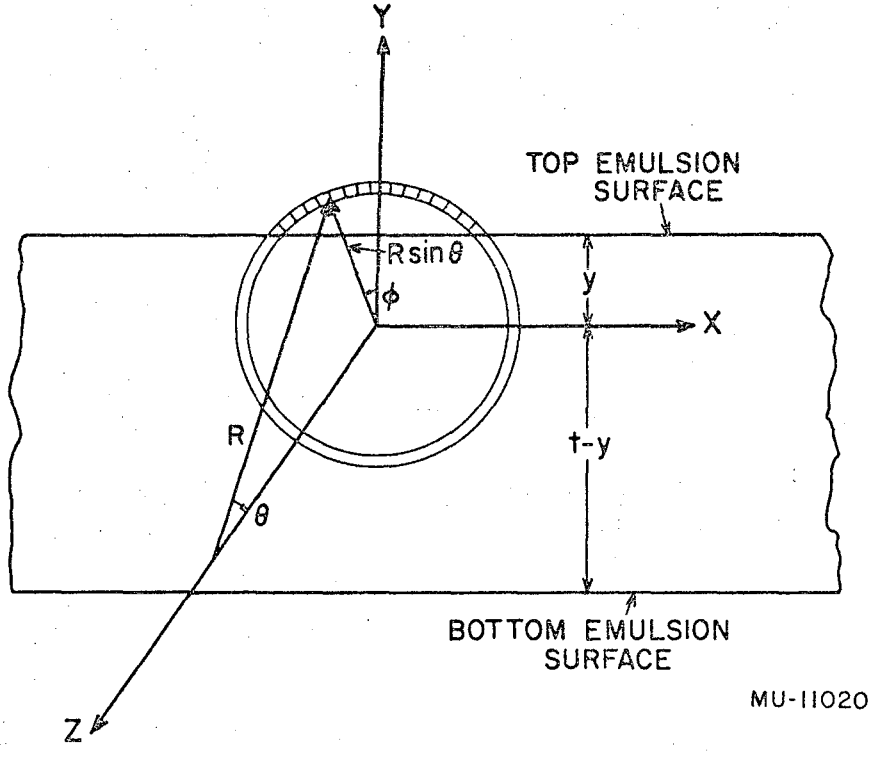

Fig. 23. Diagram for calculating the fraction of tracks of range R that leave an emulsion of thickness t within a cone of half angle θ_m. See text for further explanation.

Similarly, the number of tracks that leave the bottom emulsion surface is given by

$$\Delta N_{bottom} dy d\theta = \frac{N_0(E_n)}{\pi t} \sin 2\theta \, d\theta dy \, \cos\theta^{-1}(t-y/R \sin\theta)$$

$$\text{for } R \sin\theta > t-y \qquad (31)$$

The total number of recoils of range R that leave the emulsion between the angles θ and $\theta+d\theta$ is obtained by integrating Eq. (31) over dy:

$$\Delta N(R, \theta, t)\, d\theta = \frac{N_0(E_n)}{\pi t}\left[\int_0^{R \sin\theta} \cos^{-1}(y/R \sin\theta)\, dy + \int_{t-R\sin\theta}^{t} \cos\left[(t-y)/R \sin\theta\right] dy\right], \qquad (32)$$

which gives

$$\Delta N(R, \theta, t)\, d\theta = \frac{2 N_0(E_n)\, R}{\pi t} \sin\theta \sin 2\theta \, d\theta. \qquad (33)$$

As the correction for the tracks that leave the emulsion is to be applied to the yield of recoils per neutron energy interval, it is more convenient to express the recoil range R in terms of the neutron energy E_n that produced the recoil. In a small energy interval the range-energy relation for protons in emulsion may be represented by Eq. (25). Substitution of Eq. (10) into Eq. (25) gives

$$R = K(E_p) \cos^3\theta \, E_n^{3/2}. \qquad (34)$$

Substituting this expression for R into Eq. (33) allows the integration of Eq. (33) over $d\theta$. The number of proton recoils of range R that leave an emulsion of thickness t within a cone of half angle θ_M is then

$$\Delta N(R, \theta_M, t) = \frac{2 N_0(E_n)\, K(E_p)\, E_n^{3/2}}{\pi t} \int_0^{\theta_M} \sin\theta \sin 2\theta \cos^3\theta \, d\theta. \qquad (35)$$

The total number of proton recoils in a cone of half angle θ_M is obtained by integrating Eq. (29), with the result

$$N(E_n, \theta_M) = N_0(E_n) \frac{1}{2}\left[1 - \cos^2 \theta_M\right]. \tag{36}$$

The fraction of recoils produced by neutrons of energy E_n that leave an emulsion of thickness t through a cone of half angle θ_M is obtained by dividing Eq. (35) by Eq. (36):

$$f(E_n, \theta_M, t) = \frac{4K(E_p)\, E_n^{3/2}}{\pi t(1 - \cos^2\theta_M)} \int_0^{\theta_M} \sin\theta \sin 2\theta \cos^3\theta \, d\theta. \tag{37}$$

Finally, $K(E_p)$ may be put in terms of the neutron energy by finding the average value of E_p in a cone of half angle θ_M due to the neutrons of energy E_n:

$$\bar{E}_p = \frac{\int_0^{\theta_M} E_n \cos^2\theta \sin 2\theta \, d\theta}{\int_0^{\theta_M} \sin 2\theta \, d\theta} = \left[\frac{1 - \cos^4\theta_M}{1 - \cos^2\theta_M}\right] E_n. \tag{38}$$

For $\theta_M = 20^\circ$, Eq. (38) gives $E_p = 0.94\, E_n$ and Eq. (37) gives

$$f(E_n, 20^\circ, t) = \frac{0.128\, R(0.94\, E_n)}{t}. \tag{39}$$

Equation (39) gives the fraction of proton recoils produced by neutrons of energy E_n that leave an emulsion of thickness t within a 20° cone. Eq. (39) is plotted in Fig. 24 for an emulsion thickness of 185 microns.

The assumption of rectilinear ranges somewhat underestimates the loss of tracks. Rosen[29] gives an empirical method for estimating the actual loss. According to Rosen, the loss of 12-Mev protons from a 200-μ emulsion through a 15° cone is some 5% higher than predicted on the basis of rectilinear ranges. His results also indicate that the difference between his empirical method for determining losses and the predictions assuming rectilinear ranges become smaller as the

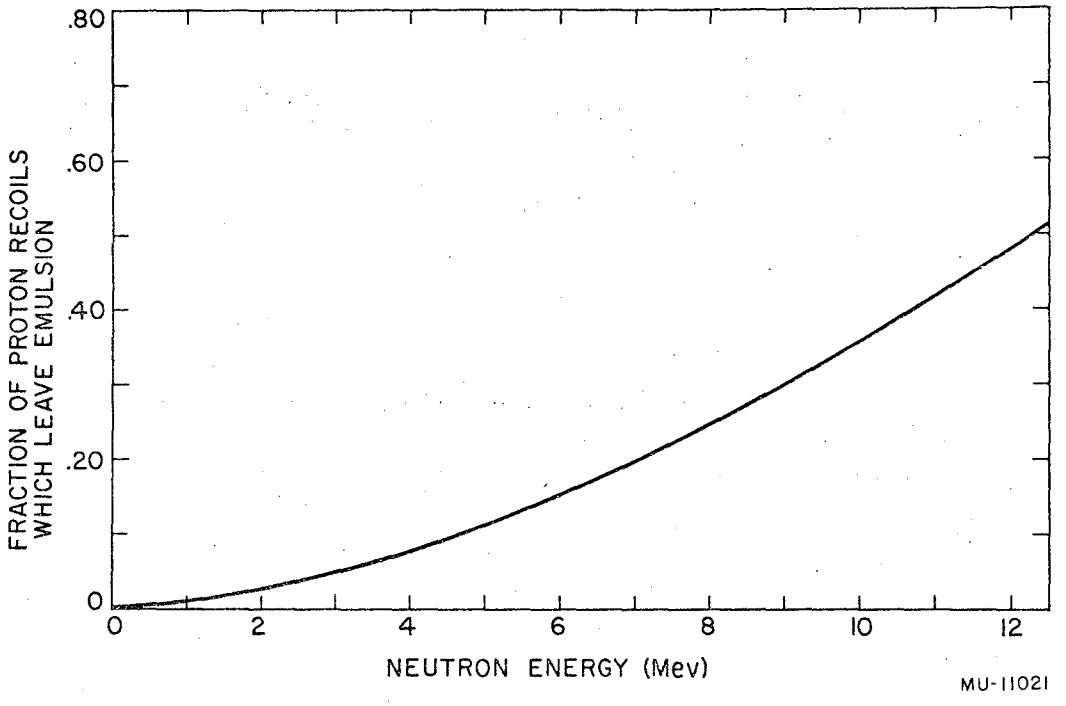

Fig. 24. The fraction of proton recoils lost from a 185-μ emulsion through a 20° cone as a function of neutron energy according to Eq. (37).

cone used becomes larger. The actual losses of recoils out of a 20° cone should not be more than a few percent greater than predicted by Eq. (39) for protons up to 12 Mev.

4. Correction for Elastic Scattering

Let

$$\frac{dN_{np}(E_n)}{dE_n}$$

be the number of neutrons per cm^2 between energies E_n and $E_n + dE_n$ at the position of detection. Consider those neutrons that go into the brass shielding and scatter at a distance r_{st} from the target. The flux of neutrons at this point would be

$$\left(\frac{r_{et}}{r_{st}}\right)^2 \frac{dN_{np}}{dE_n} (E_n)$$

but some neutrons have been absorbed and some have been scattered in going through r_{os} centimeters of shielding (see Fig. 25). Let λ_t be the mean free path for the loss of neutrons by absorption and by scattering to angles greater than 35°. The differential elastic-scattering cross section becomes small enough at this angle so that scatterings greater than 35° may be considered as lost.[32] The mean free path, as well as the neutron flux, is dependent on the neutron energy, but this specification will be henceforth dropped. The flux of neutrons per Mev at a distance r_{st} from the target and after traveling through r_{os} of shielding is then

$$\left(\frac{r_{et}}{r_{st}}\right)^2 \frac{dN_{np}}{dE_n} e^{-r_{os}/\lambda_t}.$$

To reach the emulsion by a single scattering, the neutrons must scatter by an angle ψ. It is assumed that subsequent scatterings scatter as many neutrons into the emulsion as they scatter out of it. If $\frac{d\sigma}{d\Omega}(\psi)$ is the differential elastic-scattering cross section and N_s the number of scattering centers per cm^3, then

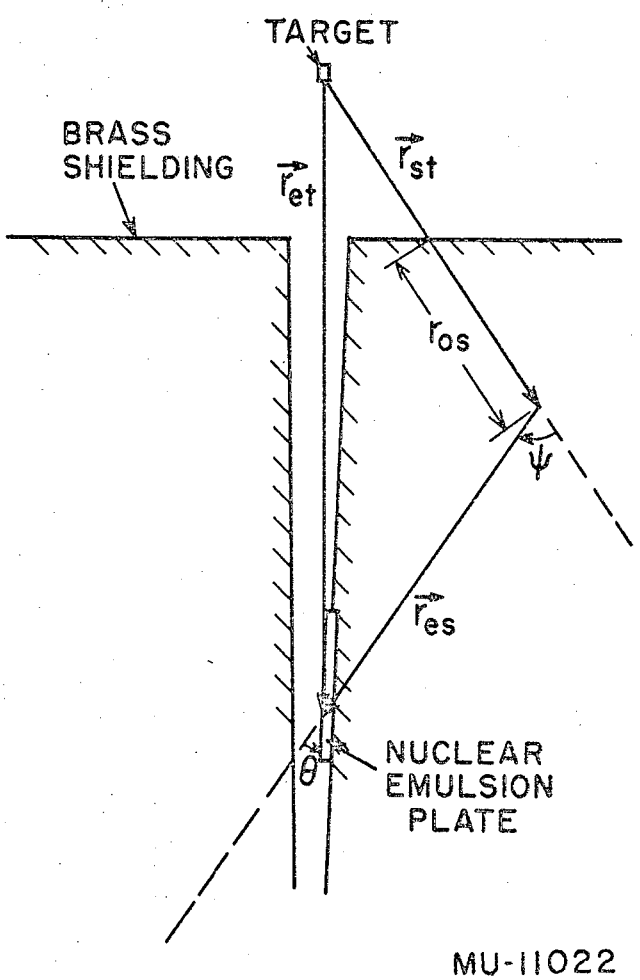

Fig. 25. Diagram illustrating the method used to correct for the elastic scattering of neutrons from the shielding. See text for further explanation.

$$\left(\frac{r_{et}}{r_{st}}\right)^2 \frac{dN_{ne}}{dE_n} \cdot e^{-r_{os}/2t} N_s \frac{d\sigma}{d\Omega}(\psi)$$

is the number of neutrons per Mev that are scattered an angle ψ, per steradian by 1 cm^3 of scatterer after traversing r_{os} of scatterer. The detector subtends a solid angle

$$\frac{\Delta A}{r_{es}^2} \sin\theta$$

to this scattered flux, where ΔA is the emulsion area scanned, θ is the angle between the scattered flux and the emulsion surface, and r_{es} is the distance between the point of scattering and the point of detection. By the time this scattered flux has reached the point of detection, it has again been attenuated by the amount e^{-r_{os}/λ_t}. The number of neutrons per Mev scattered by the 1 cm^3 of shielding specified above, and that reach the emulsion of area ΔA, is then

$$\frac{dN_{ns}}{dE_n} = \left(\frac{r_{et}}{r_{st}}\right)^2 \frac{dN_{ne}}{dE_n} e^{-r_{os}/\lambda_t} N_s \frac{d\sigma}{d\Omega}(\psi) \frac{\Delta A}{r_{es}^2} \sin\theta e^{-r_{os}/\lambda_t}. \quad (40)$$

The probability that one of these scattered neutrons produces a proton recoil into the solid angle $\Delta\Omega$ at the angle θ to the scattered flux is given by Eq. (2) as

$$\rho_p \sigma_{np} \frac{t_e}{\sin\theta} \cos\theta \Delta\Omega,$$

where ρ_p is the number of protons per cm^3 of emulsion, $\cos\theta\,\Delta\Omega$ assumes a spherical symmetry for n-p collisions in their center of mass, and the other quantities are the same as specified in Eq. (2).

The number of proton recoils per Mev of neutron energy produced by the scattered flux $\frac{dN_{ns}}{dE_n}$ is then

$$\frac{dN_{sp}}{dE_n} = \left(\frac{r_{et}}{r_{st}\, r_{es}}\right)^2 e^{-\frac{r_{os} + r_{es}}{\lambda_t}} N_s \cos\theta \, \frac{d\sigma}{d\Omega}(\psi) \, \frac{dN_{ne}}{dE_n} \rho_p t_e \, \Delta A \Delta\Omega \sigma_{np}. \quad (41)$$

However, the quantity

$$\frac{dN_{ne}}{dE_n} \rho_p t_e \, \Delta A \Delta\Omega \, \sigma_{np},$$

when compared to Eq. (2), is just the number of proton recoils produced by the primary flux at the emulsion into the solid angle $\Delta\Omega$ and within the emulsion volume $t_e \Delta A$. Therefore the ratio of proton recoils due to the scattered neutrons from 1 cm^3 of shielding to the proton recoils due to the primary flux per Mev of neutron energy is

$$f(\vec{r}_{et}, \vec{r}_{se}, E_n) = \left(\frac{r_{et}}{r_{st}\, r_{es}}\right)^2 N_s \, e^{-\frac{r_{os} + r_{es}}{\lambda_t}} \cos\theta \, \frac{d\sigma}{d\Omega}(\psi), \quad (42)$$

where the position of the scatterer is determined by $\vec{r}_{et}$ and $\vec{r}_{se}$. The shielding was divided into elementary volumes of 1 cm^3 each, starting with the median plane, and the quantity f was evaluated for each cm^3 of scatterer. The distances and angles were measured with respect to the center of each cm^3 of shielding and the elastic-scattering cross sections and mean free paths were obtained from information in the literature.[31, 32, 33] Because of the peaking of elastic scattering at small angles, the largest contribution to the scattered neutron flux comes from the material that allows neutrons to reach the detector by a small-angle elastic scatter. Unfortunately, this is the same material as is required to reduce the charged-particle background.

The summation of the quantities f is the ratio of the proton recoils due to the scattered neutron flux to the proton recoils due to the primary flux for neutrons of energies between E_n and $E_n + dE_n$. However, since the scattered neutron flux makes an angle θ to the emulsion surface, the resulting proton recoils have smaller ranges than the proton recoils due to the primary flux, which is parallel to the emulsion surface. From a knowledge of the quantities f one can calculate the average value of $\cos^2\theta$ by

$$\overline{\cos^2\theta} = \frac{\Sigma \cos^2\theta\, f(\theta)}{\Sigma f(\theta)} . \tag{43}$$

The average proton energies made by elastically scattered neutrons of energy E_n is given by Eq. (10) to be

$$\overline{E_p} = E_n \overline{\cos^2\theta} . \tag{44}$$

If $N_0(E_n)$ is the observed number of neutrons of energy E_n, it is related to the number of primary neutrons $N_P(E_n)$ by

$$N_0(E_n) = N_P(E_n) + f(E_n \overline{\cos^2\theta})\, N_P(E_n \cos^2\theta). \tag{45}$$

Assuming the spectral shape given by simple evaporation theory (Eq. (13)), we have the number of primary neutrons corrected for elastic scattering given by

$$N_P(E_n) = \frac{N_0(E_n)}{\left[1 + \cos^2\theta\, f(E_n \overline{\cos^2\theta})\, e^{-(\overline{\cos^{-2}\theta}-1)\, E_n/T}\right]} . \tag{46}$$

5. Center-of-Mass Motion

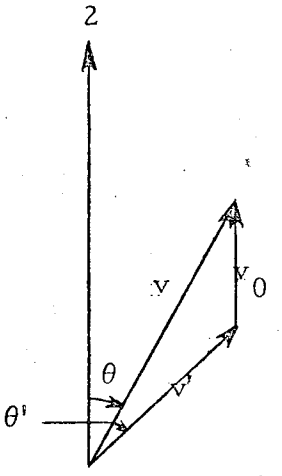

Fig. 26

A particle has the velocity v' at the angle θ' in the center-of-mass system. Assume that the center of mass is moving with the velocity v_0 in the z direction (see Fig. 26). The particle is observed in the laboratory system at the angle θ with the velocity v. Concerning energy and momentum, we find that the particle velocity in the center-of-mass system v' is related to the laboratory velocity, v, by

$$v' = \left[v^2 + v_0^2 - 2 v v_0 \cos\theta \right]^{1/2} . \tag{47}$$

the center-of-mass angle θ' is related to the laboratory angle θ by

$$\cos\theta' = \frac{v \cos\theta - v_0}{v'} . \tag{48}$$

From the transformation properties of solid angle and of energy it can be shown that the laboratory-system differential cross section, $\frac{d\sigma'}{d\Omega' dE'}(E', \theta')$, by

$$\frac{d\sigma}{d\Omega dE}(E, \theta) = \frac{v}{v'} \frac{d\sigma'}{d\Omega' dE'}(E', \theta') = \left(\frac{E}{E'}\right)^{1/2} \frac{d\sigma'}{d\Omega' dE'}(E', \theta'). \tag{49}$$

The relation between E' and E can be obtained from Eq. (47):

$$E' = E + \frac{R_n}{2} \beta_0^2 - (2 R_n E)^{1/2} \beta_0 \cos\theta, \tag{50}$$

where R_n is the rest mass in Mev of the detected particle and β_0 is the center-of-mass velocity in units of the velocity of light.

Equation (49), together with the angular distributions, may be used to obtaine β_0. If β_0 is small compared with the β of the detected particle, then the angular distribution observed at 90° is essentially the distribution in the center-of-mass system, $\frac{d\sigma'}{d\Omega' dE'}(E')$. assuming that the center-of-mass distribution is isotropic. Points are found on the 135° and 90° data that satisfy Eq. (49), and the resulting β_0 may be calculated from Eq. (50). The same procedure may be used to find a β_0 from comparison of the 45° and 90° data. If the observed distribution is the result of a center-of-mass motion of an evaporating nucleus, then the β_0's should all be the same. The data at the three angles can reasonably be explained by β_0's of about 0.014, 0.012, and 0.010 for carbon, aluminum, and nickel, respectively, in the neutron energy interval 0.5 to 1.0 Mev. These represent about 30%, 60%, and 100% momentum transfers to the struck carbon, aluminum, and nickel nuclei respectively. These center-of-mass velocities are expected to be somewhat overestimated because of the presence of cascade neutrons; however, they are in agreement with the center-of-mass velocities estimated by Bailey.[15] Above a neutron energy of 1 Mev, the same β_0's fit the 90° and 135° data up to a neutron energy of about 3 Mev. Beyond 3 Mev, the β_0 necessary to fit the 90° and 135° data increases with increasing neutron energy. At a neutron energy of about 5 Mev, the β_0 required to fit the 90° and 135° data for carbon and aluminum represents a momentum for the evaporating nucleus that is greater than the momentum of the bombarding proton.

BIBLIOGRAPHY

1. E. Bagge, Ann. Physik 39, 535 (1941).
2. R. Serber, Phys. Rev. 72, 1114 (1947).
3. M.L. Goldberger, Phys. Rev. 74, 1269 (1948).
4. Bernardini, Booth, and Lindenbaum, Phys. Rev. 88, 1017 (1952)
5. H. McManus and W.T. Sharp, private communication to W. Heckrotte.
6. V. Weisskopf, Phys. Rev. 52, 295 (1937).
7. L. Wolfenstein, Phys. Rev. 82, 690 (1951).
8. E. Bagge, Ann. Physik 33, 389 (1938).
9. K.J. LeCouteur, Proc. Phys. Soc. A63, 259 (1950).
10. Harding, Lattimore, and Perkins, Proc. Roy. Soc. A196, 325 (1949).
11. D.H. Perkins, Phil. Mag. 41, 138 (1950).
12. Bernardini, Booth, and Lindenbaum, Phys. Rev. 85, 826 (1952).
13. Lock, March, and McKeague, Proc. Roy. Soc. A231, 368 (1955).
14. P.C. Gugelot, Phys. Rev. 93, 425 (1954).
15. L.E. Bailey, "Angle and Energy Distributions of Charged Particles from the High-Energy Nuclear Bombardment of Various Elements, "University of California Radiation Laboratory Report No. UCRL-3334.
16. P.C. Gugelot, Phys. Rev. 81, 51 (1951).
17. E.R. Graves and L. Rosen, Phys. Rev. 89, 343 (1953).
18. D.M. Skyrme and W.S.C. Williams, Phil. Mag. 42, 1187 (1951).
19. J.A. Hofmann and K. Strauch, Phys. Rev. 90, 449 (1953).
20. Warren F. Stubbins, "An Experimental Ion Source for the 184-Inch Cyclotron," University of California Radiation Laboratory Report No. UCRL-2698, Feb. 1, 1955.
21. C.F. Powell and G.E.F. Fertel, Nature 144, 115 (1939).
22. R.K. Adair, Revs. Modern Phys. 22, 249 (1950).
23. Crandall, Millburn, Pyle, and Birnbaum, Phys. Rev. 101, 329 (1956).

BIBLIOGRAPHY (Cont.)

24. Francis C. Gilbert, "Analysis of the Disintegration Products from the Reactions of 125-Mev Deuterons with Lithium Nuclei," University of California Radiation Laboratory Report No. UCRL-2771, Oct. 15, 1954.
25. J. Rotblat and C. T. Tai, Nature 164, 835 (1949).
26. C. Waller, private communication.
27. A. J. Oliver, Rev. Sci. Instr. 25, 326 (1954).
28. W. H. Barkas and D. M. Young, "Emulsion Tables. I. Heavy-Particle Functions," University of California Radiation Laboratory Report No. UCRL-2579 (rev.), Sept. 1954.
29. L. Rosen, Nucleonics 11, 38 (August 1953).
30. I. Hamouda and G. deMontmollin, Phys. Rev. 83, 1277 (1951).
31. H. H. Barschall and R. F. Taschek, Phys. Rev. 75, 1819 (1949).
32. N. Nereson and F. Reines, Rev. Sci. Instr. 21, 534 (1950).
33. J. J. Wilkins, "Range-Energy Relations for Ilford Nuclear Emulsion," Report AERE-G/R-664, Harwell (1951).
34. M. Walt and H. H. Barschall, Phys. Rev. 93, 1062 (1954).
35. M. Walt and J. R. Beyster, Phys. Rev. 98, 677 (1955).
36. Taylor, Lonsjo, and Bonner, Phys. Rev. 100, 174 (1955).
37. J. M. Blatt and V. F. Weisskopf, "Nuclear Physics," New York, Wiley, 1952, p. 348.
38. K. J. LeCouteur, Proc. Phys. Soc. A65, 718 (1952).
39. D. A. Hicks and A. J. Kirschbaum, "Total Attenuation Cross Sections for High-Energy Protons," Livermore Research Laboratory, MTA-28, May 1953.
40. Batzel, Miller, and Seaborg, Phys. Rev. 84, 671 (1951).
41. W. E. Nervik and G. T. Seaborg, Phys. Rev. 97, 1092 (1955).
42. Fermi, Orear, Rosenfeld, and Schluter, "Nuclear Physics," Chicago University of Chicago Press, 1950, p. 6.
43. W. H. Barkas, Phys. Rev. 55, 691 (1939).
44. J. M. Wilcox and B. J. Moyer, Phys. Rev. 99, 875 (1955).
45. D. M. Skyrme, private communication.